CONF-9506249--1

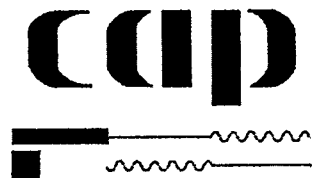

BNL-62048
CAP 129-95R

Far Field Acceleration

Richard C. Fernow
Brookhaven National Laboratory, Upton, NY

JULY 1995

CENTER FOR ACCELERATOR PHYSICS

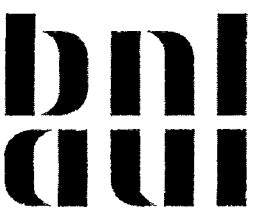

BROOKHAVEN NATIONAL LABORATORY
ASSOCIATED UNIVERSITIES, INC.

Under Contract No. DE-AC02-76CH00016 with the
UNITED STATES DEPARTMENT OF ENERGY

Lectures: Adv. Accel. Phys. School, IHEP, Beijing, China, 6/14-17/95

DISCLAIMER

This report was prepared as an account of work sponsored by an agency of the United States Government. Neither the United States Government nor any agency thereof, nor any of their employees, nor any of their contractors, subcontractors, or their employees, makes any warranty, express or implied, or assumes any legal liability or responsibility for the accuracy, completeness, or usefulness of any information, apparatus, product, or process disclosed, or represents that its use would not infringe privately owned rights. Reference herein to any specific commercial product, process, or service by trade name, trademark, manufacturer, or otherwise, does not necessarily constitute or imply its endorsement, recommendation, or favoring by the United States Government or any agency, contractor or subcontractor thereof. The views and opinions of authors expressed herein do not necessarily state or reflect those of the United States Government or any agency, contractor or subcontractor thereof.

DISCLAIMER

Portions of this document may be illegible in electronic image products. Images are produced from the best available original document.

BNL-62048

Far field acceleration

Richard C. Fernow

Physics Department
Brookhaven National Laboratory

Lectures presented at the Advanced Accelerator Physics School
IHEP, Beijing, China, June 14-17, 1995

Far fields are propagating electromagnetic waves far from their source, boundary surfaces, and free charges. The general principles governing the acceleration of charged particles by far fields are reviewed. A survey of proposed field configurations is given. The two most important schemes, Inverse Cerenkov acceleration and Inverse free electron laser acceleration, are discussed in detail.

DISTRIBUTION OF THIS DOCUMENT IS UNLIMITED

MASTER

Contents

Chapter 1 Overview of far field acceleration

1.1 Definition of a far field

A far field is an electromagnetic field that can be expressed as a sum of propagating electromagnetic waves

$$\vec{E}(\vec{x},t) = \sum_j A_j \exp[i(\vec{k}_j \cdot \vec{x}_j - \omega_j t)] \tag{1.1}$$

where the k_j are the wavevectors of real, transversely polarized waves. Fields with imaginary k_j are called *near fields*. The far fields have a harmonic time dependence. We are ultimately interested in the interaction of a charged particle with the far fields. If we define d to be a characteristic dimension of the interaction region, λ the wavelength of the far field, and R the distance from the source of the far fields or from other boundary surfaces, then we will require that the inequalities $R \gg \lambda$, d be satisfied. Otherwise, near field effects may be important.

There has been interest in using far fields for acceleration because very high electric fields can be created using a focused laser beam [1-9]. It may be possible to achieve accelerating gradients of 1 GeV/m using this method, compared to 50 MeV/m using conventional rf acceleration. This might allow building TeV-level linear colliders of much smaller size or table top GeV-scale accelerators. The very strong fields might also be used to make very strong focusing elements with gradients of ~1000 T/m, compared to ~100 T/m for conventional superconducting quadrupoles.

1.2 General principles governing acceleration using far fields

A charged particle in an electromagnetic field (E, B) must satisfy the equations of motion

$$\begin{aligned} mc\frac{d}{dt}(\gamma\vec{\beta}) &= e(\vec{E} + c\vec{\beta}\times\vec{B}) \\ mc^2\frac{d}{dt}(\gamma) &= ec(\vec{\beta}\cdot\vec{E}) \end{aligned} \tag{1.2}$$

where m is the particle mass, e is the particle charge, γ is the relativistic energy factor, β is the relativistic velocity and c is the speed of light in vacuum. The second equation shows that in order to increase its energy, the particle must have a component of velocity along E. We are interested in the following in acceleration mechanisms that maintain synchronism of the phase between the particle and the wave. Thus, we are not interested in"one shot" mechanisms. We distinguish two types of acceleration processes.

A *first order* process is one where the particle interacts with one wave, such that

$$\frac{dE}{dz} \propto e\, v_z\, E_z^{(1)} \tag{1.3}$$

In a *second order* process the particle must interact with two waves. One wave gives the particle a component of transverse velocity

$$v_T \propto e \left\{ \begin{matrix} E^{(2)} \\ B^{(2)} \end{matrix} \right\}$$

Then the particle can gain energy by interacting with the transverse component of the electric field

$$\frac{dE}{dz} \propto e\, v_T\, E_T^{(1)}$$

so that the combined interaction is given by

$$\frac{dE}{dz} \propto e^2\, E_T^{(1)} \left\{ \begin{matrix} E^{(2)} \\ B^{(2)} \end{matrix} \right\} \tag{1.4}$$

Note that the second order process is proportional to e^2 and thus works simultaneously on both signs of particle charge. The first order process is proportional to e and cannot accelerate both signs of charge at the same phase.

In discussions of far field acceleration we consider the source of radiation to be located a great distance from the interaction region. The particle travels either in a vacuum or in a static medium, which we define as a medium that only contains charges bound in a dielectric. Static media are characterized by a dielectric constant or by a refractive index n. We do not consider the case when free charges are present in the medium (e.g plasma acceleration). The charges in a static medium cannot move in response to the externally applied far field. In the quantum viewpoint far field acceleration takes place through the exchange of real (not virtual) photons.

Far field acceleration schemes offer several advantages over other laser acceleration schemes. The interaction occurs a large distance from any material boundaries. Thus we can try to use the very large electric field that is present at a focus. In a vacuum there are no breakdown problems from nearby boundary surfaces and no plasma formation. There are also no limitations on particle intensities due to wakefields induced in boundary surface walls.

On the other hand, there are also several disadvantages of using far field acceleration. Since we are dealing with real, propagating electromagnetic waves, the electric field is perpendicular to the direction of propagation of the wave. This makes it impossible to fully utilize the large electric field in the focus for acceleration. If the propagation directions of the wave and particle are parallel, there is no acceleration because $\beta \perp E$. If the propagation directions make a small angle θ, the interaction strength will be proportional to $E_o\theta$. If the angle between the wave and particle is made large, the interaction strength becomes large, but the total distance over which the interaction takes place becomes small. Many second order schemes increase the interaction strength by giving the particle an oscillating transverse component of velocity. Although this scheme works well at low velocities, the acceleration gradients decrease as the particle approaches relativistic velocities. Using a focused laser spot to achieve a high field strength also implies that the accelerator must be made up of a series of finite interaction regions, separated by regions where the light is regenerated or refocused.

Consider a particle travelling with velocity βc in a vacuum along the z axis, as shown in Fig. 1.1. A wave crosses the particle trajectory at an angle θ. The phase velocity of the wave is

$$v_P = \frac{\omega}{k_Z} = \frac{c}{\cos(\theta)} > c \tag{1.5}$$

In order to get continuous interaction the phase velocity of the wave has to equal the velocity of the particle. Thus this is not possible in a vacuum. However, it is possible to reduce the phase velocity of the wave by using a dielectric medium.

$$v_P = \frac{\omega}{n k_Z} = \frac{c}{n \cos(\theta)} \tag{1.6}$$

In this case synchronism is possible, provided

$$\cos(\theta) = \frac{1}{\beta n} \tag{1.7}$$

This is the same relation that occurs for Cerenkov radiation, so acceleration under these conditions is referred to as inverse Cerenkov acceleration or ICA. This is the only example of a first order, far field acceleration process.

All other far field acceleration schemes are second order processes. A second field is used to give the particle an oscillating component of transverse velocity. Consider in Fig. 1.2 a coherent radiation wavefront at AB. Let the particle travel to the right between A and O, one period D apart.

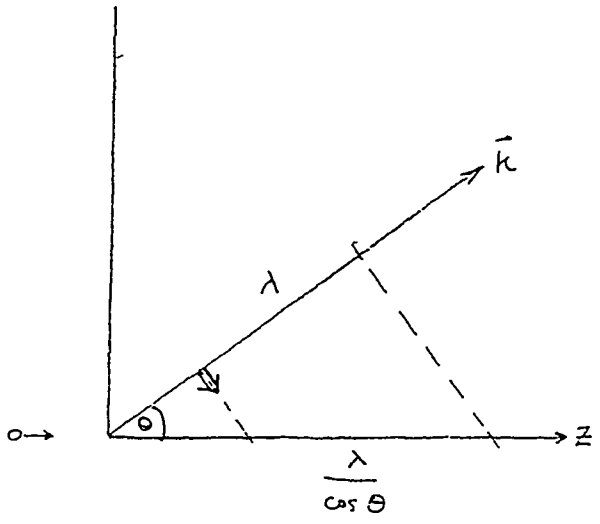

Fig. 1.1 A particle and a plane wave crossing in a vacuum

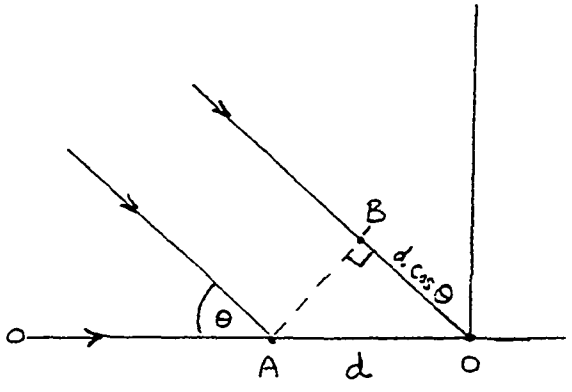

Fig. 1.2 Second order synchronism relation

The particle can interact synchronously with the incoming wave front if the time for the particle to get from A to O differs by an integer number of radiation periods from the time for the wave to get from B to O.

$$\frac{D}{\beta_z c} - \frac{D\cos(\theta)}{c} = m\frac{\lambda}{c} \tag{1.8}$$

where m is an integer. We take m = 1 for the rest of this paper. In other words synchronism can be maintained provided the particle slips one radiation wavelength behind the wave in each period of the particle's motion. The most important example of this type of acceleration scheme is the inverse free electron laser or IFEL.

1.3 Considerations for useful far field accelerators

The usefulness of a far field acceleration scheme depends of course on the specific application. However, since many acceleration techniques are already known, most research in this area has emphasized achieving large accelerating gradients. Besides this, we are interested here in schemes that are capable of continuous acceleration of relativistic particles and thus exclude "one shot" acceleration methods. Techniques that exhibit symmetry in the fields are highly desirable since they can provide a neutral axis where the particle is free of deflecting forces. In addition a practical accelerator must provide reasonable values of repetition rate, pulse length, energy spread, transverse emittance, and intensity.

For applications to colliding beam accelerators a parameter of great importance is the luminosity

$$L = \frac{N^2 f \gamma}{4\pi\beta^* \epsilon_N} \tag{1.9}$$

where N is the number of particles per bunch, f is the repetition frequency, β^* is betatron oscillation amplitude at the collision point, and ε_N is the normalized transverse emittance. Any acceleration scheme using lasers will be forced into an unconventional choice of parameters in order to achieve high luminosities. Because of the very short wavelength of the radiation, N must be smaller here than for conventional colliders or else space-charge effects will be extremely large. γ is fixed by physics requirements and ε_N is determined by source parameters. Thus to recover the luminosity, laser accelerators must operate with higher values of f / β^*.

Consider now a laser beam focused by a lens characterized by an f-number $f_\#$ (= focal length / lens diameter). The radius w_0 of the focused spot can be determined from the size of the Airy disk in diffraction theory

$$w_o \simeq 1.22\, \lambda f_\# \tag{1.10}$$

The depth of focus is

$$z_R \simeq 2\, \lambda f_\#^2 \tag{1.11}$$

In the theory of gaussian optics the radius of the e^{-2} irradiance contour varies with the distance z from the focal plane as

$$w(z) = \left\{ 1 + \left(\frac{z}{z_R} \right)^2 \right\}^{1/2} \tag{1.12}$$

The *Rayleigh range* is given by

$$z_R = \frac{\pi w_o^2}{\lambda} \tag{1.13}$$

The cross sectional area of the beam doubles at $\pm z_R$. Far from the focal plane the beam diverges at an angle

$$\theta = \frac{\lambda}{\pi w_o} \tag{1.14}$$

The radius of curvature of the wavefront is given by

$$\rho(z) = z \left[1 + \left(\frac{z_R}{z} \right)^2 \right] \tag{1.15}$$

The wavefront is flat ($\rho \rightarrow \infty$) at the focal plane and at ∞. The radius ρ has a minimum at some intermediate value of z.

The electric field at the focus can be determined from the Poynting vector

$$\vec{S} = \vec{E} \times \vec{H} \tag{1.16}$$

where S has the dimensions of power per area. For far fields E is perpendicular to H and in-phase.

If we consider the time average of S over one period, we find that the peak magnitude of the electric field is

$$E_P = \sqrt{2 Z_o S} \tag{1.17}$$

where $Z_o \approx 377\ \Omega$ is the impedance of free space. As an example, if we consider a 1 TW YAG laser ($\lambda \approx 1\ \mu m$), the power density is $3\ 10^{23}\ W / m^2$ and the peak electric field is around $10^{13}\ V / m$.

An important issue for a practical accelerator is how the individual interaction regions are connected together to form the total accelerator. This is referred to as staging. Fig. 1.3 shows two possible scenarios. In the first unused power from the first interaction region is refocused and then used for the second and so on. Problems here include how to transmit the very high laser power without damage and the fact that each succeeding station sees a reduced amount of laser power. The second alternative approach is to feed all the sections in parallel. This would require many more laser amplifiers, all of which would have to maintain phase coherence with the driver signal.

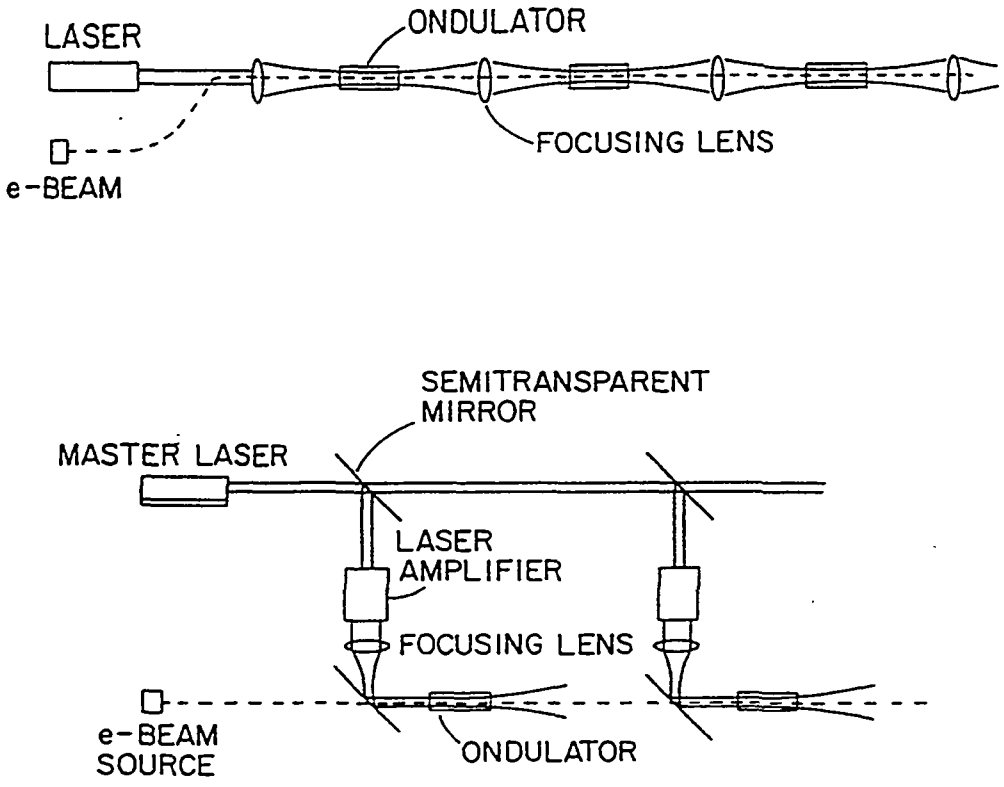

Fig. 1.3 Possible configurations for staging acceleration sections [1].

The actual electromagnetic field in a focus is quite complicated [10]. Consider a plane wave incident on a lens as illustrated in Fig. 1.4. The lens in parameterized by its focal length f and its convergence angle α . The x-y plane is the focal plane of the lens. Fig. 1.5 shows contours of the electric field energy density plotted in terms of the variables

$$u = kz\sin^2(\alpha)$$
$$v = k\sqrt{x^2 + y^2}\sin(\alpha)$$

One can see that the integrated fields encountered by a particle travelling $-\lambda$ off the optical axis will differ considerably from the fields seen by a particle on the axis. It is also important to note that significant longitudinal components of E exist near the focal plane, and these can act to destroy any phase synchronization.

1.4 Motion of a charged particle in an electromagnetic wave

Consider an isolated charged particle acted upon by a propagating plane electromagnetic wave [11-12]. The wave exerts electric and magnetic forces on the particle according to Eq. 1.2. A particle, initially at rest, gets a transverse component of velocity from the E field. The transverse velocity then interacts with the B field in the wave to give a longitudinal velocity. However, the plane wave cannot give the particle a net acceleration in any direction. Because of the symmetric nature of the interaction in space and time, any energy absorbed during one half-cycle of the wave must be radiated away during the next half-cycle. In the quantum viewpoint, this is equivalent to saying that energy-momentum conservation cannot be satisfied in the interaction between a free charged particle and a real photon.

If the plane wave is linearly polarized along y, the equations of motion become

$$\begin{aligned} p_X &= const \\ \frac{d}{dt}(\gamma v_Y) &= \frac{e}{m}(1 - \beta_Z)\,E_Y(z,t) \\ \frac{d}{dt}(\gamma v_Z) &= \frac{e}{m}\beta_Y E_Y(z,t) \\ \frac{d}{dt}(\gamma) &= \frac{e}{mc}\beta_Y E_Y(z,t) \end{aligned} \tag{1.18}$$

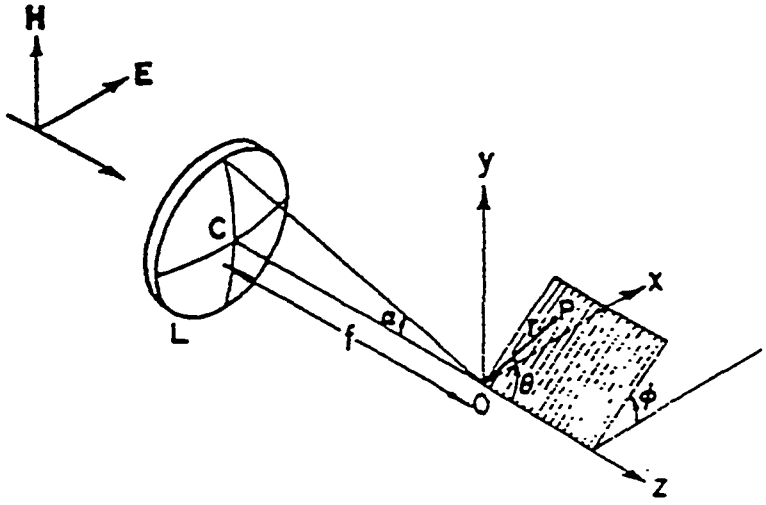

Fig. 1.4 Focal region geometry [10].

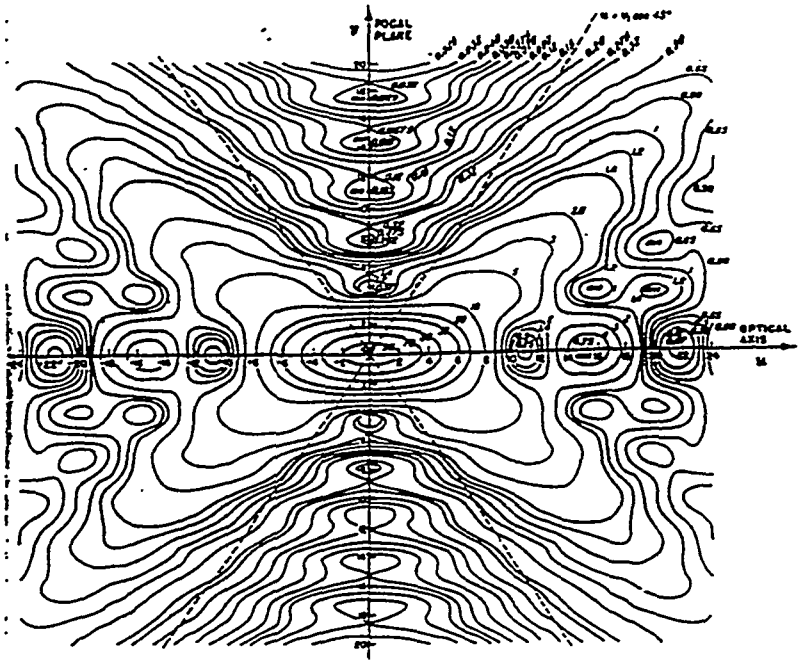

Fig. 1.5 Contours of time-averaged electric field energy density in the vicinity of the focal plane [10].

In a reference frame where the average longitudinal motion vanishes, the particle traces out a "figure 8" in the y-z plane. Fig. 1.6 shows the displacement along y and z as a function of time. The particle oscillates along y. There is a small net drift along z. This does not represent a net acceleration along z, however, because the particle velocity along z is also oscillatory. The particle interaction with the wave is often parameterized using the dimensionless wave amplitude

$$\alpha = \frac{e\,\mathrm{E}\,\lambda}{2\,\pi\,m\,c^2} \tag{1.19}$$

When $\alpha \geq 1$ the particle motion along z can continue for more than 1 period before coming back to rest.

In a circularly polarized plane wave the electric field has the form

$$\begin{aligned} \mathrm{E}_Y &= \mathrm{E}_o \cos(kz - \omega t + \Phi) = -c\,B_X \\ \mathrm{E}_X &= \mathrm{E}_o \sin(kz - \omega t + \Phi) = c\,B_Y \end{aligned} \tag{1.20}$$

The equations of motion are

$$\begin{aligned} \frac{d}{dt}(\gamma v_X) &= \frac{e}{m}(1 - \beta_Z)\,\mathrm{E}_X \\ \frac{d}{dt}(\gamma v_Y) &= \frac{e}{m}(1 - \beta_Z)\,\mathrm{E}_Y \\ \frac{d}{dt}(\gamma v_Z) &= \frac{e}{m}[\,\beta_X \mathrm{E}_X + \beta_Y \mathrm{E}_Y\,] \\ \frac{d}{dt}(\gamma) &= \frac{e}{mc}[\,\beta_X \mathrm{E}_X + \beta_Y \mathrm{E}_Y\,] \end{aligned} \tag{1.21}$$

In a reference frame where the average longitudinal motion vanishes, the particle traces out a circle in the x-y plane.

1.5 Survey of far field acceleration schemes

Far field acceleration schemes involving one or two fields are summarized in Table 1.1.

Table 1.1 Classification of far field acceleration methods

Order	Fields	Coupling	v_T	Example
1	1 EM	e	0	ICA
2	2 EM	e^2	v_{To}	Radiation pressure 2-wave IFEL
2	1 EM + static B_T	e^2	v_{To}	IFEL Inverse synchrotron radiation
2	1 EM + static E_T	e^2	v_{To}	Inverse bremsstrahlung
2	1 EM + static B_L	e^2	v_{To}	Cyclotron resonance

As we have mentioned previously, Inverse Cerenkov acceleration is the only example of a first order process. It only requires one field, has coupling proportional to e and has zero transverse velocity. ICA will be considered in Chapter 2. All the other acceleration schemes are second order. They require at least two fields, have coupling proportional to e^2, and require the particle to have a transverse velocity component. One of the fields is always an electromagnetic wave. The schemes differ in what they use for the second field [13-18]. The most promising of these methods is inverse FEL acceleration, which uses a static, transverse magnetic field to control the particles' transverse velocity. IFELA will be discussed in Chapter 3. Although we do not discuss them here, schemes have also been proposed that use more than two fields [19-20].

1.5.1 Radiation pressure

Consider a electron exposed to a wave of circularly polarized light [7]. We have seen that the electron has a circular orbit in the plane perpendicular to the wave vector, but does not achieve a net acceleration if we only consider the incident wave.

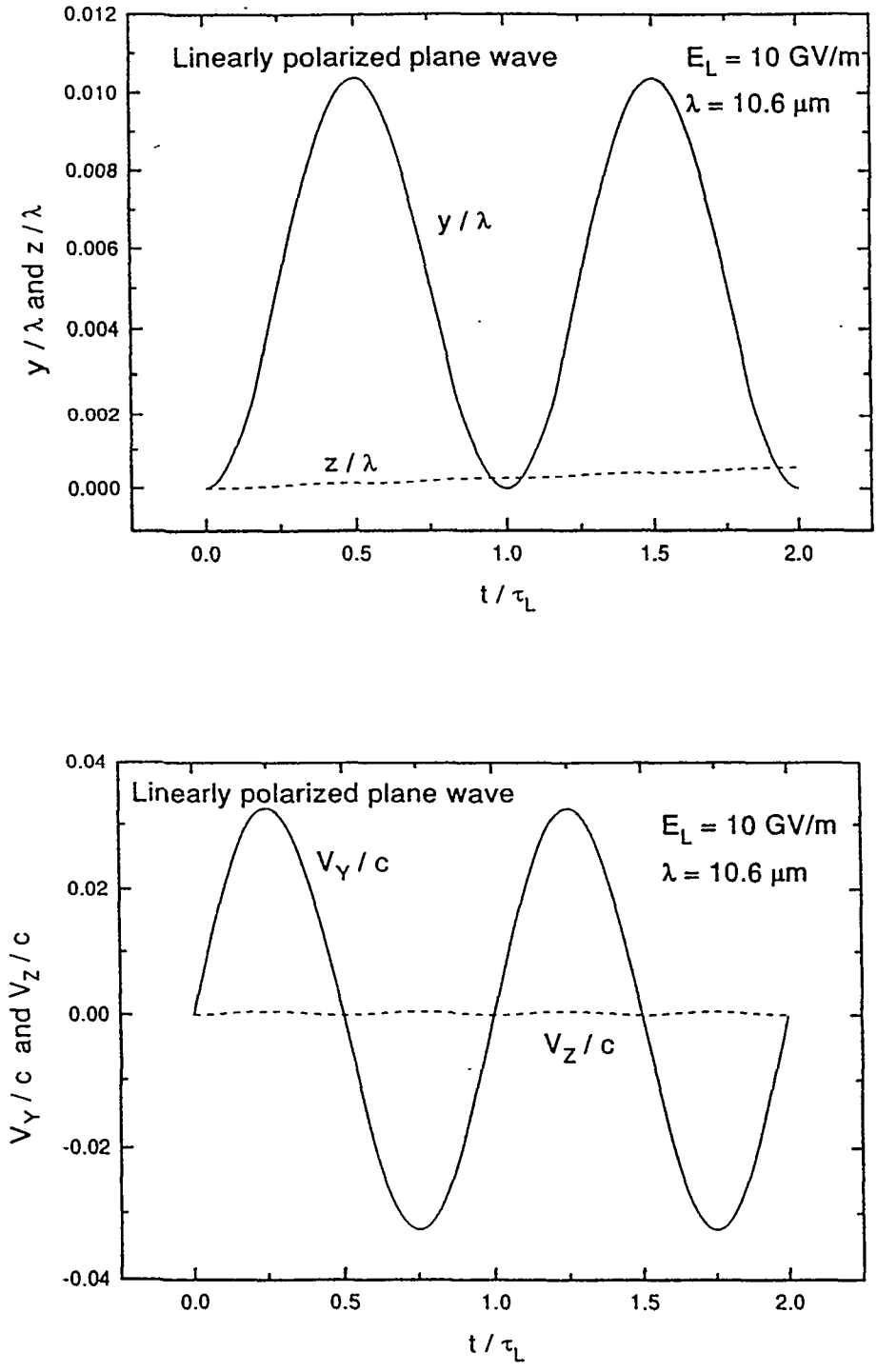

Fig. 1.6 Particle displacement and velocity in a linearly polarized plane wave as a function of time.

If we assume the electron velocity is small compared to c, then the radial force on the electron is

$$F_R = eE = \frac{mv_T^2}{\rho} = m\rho\omega^2 = m\dot{v}$$

where e is the electron charge, E is the electric field of the wave, m is the electron mass, v_T is the transverse velocity, ρ is the radius of curvature, and ω is the angular velocity. From these relations we can derive

$$\rho = \frac{eE}{m\omega^2}$$

$$v_T = \frac{eE}{m\omega}$$

$$\dot{v} = \frac{eE}{m}$$

However, because of the circular orbit, the electron will radiate the power

$$P_{rad} = \frac{2e^2\gamma^4}{3c^3}\dot{v}^2\frac{1}{4\pi\epsilon_o}$$

In the steady state the radiated power must be supplied by the work of the incident wave on the electron. This requires the existence of a phase shift between the electron position in the orbit and the wave polarization, as shown in Fig. 1.7.

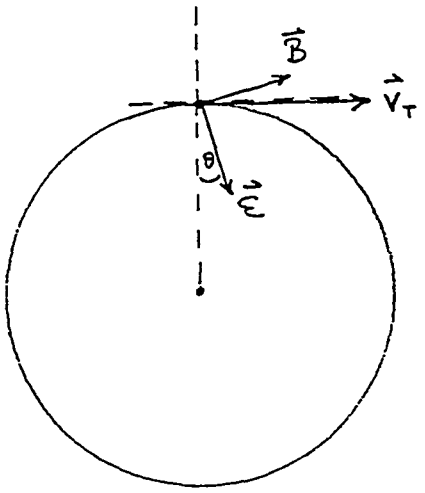

Fig. 1.7 Phase shift required by the radiation pressure interaction.

The incident power is

$$P_{inc} = e\,\mathrm{E}\,v_T \sin(\theta)$$

If we equate the incident and radiated power, we find that the phase rotation angle is

$$\theta \approx \frac{2}{3} r_e \frac{\omega}{c} \tag{1.22}$$

There is now a continuous force or energy gradient acting along z given by

$$F_Z = \frac{dE}{dz} = \frac{2}{3} e^2 \mathrm{E}^2 \frac{r_e}{mc^2} \tag{1.23}$$

Note again that a second (radiated in this case) wave was necessary in order to obtain continuous acceleration. As an example, consider a circularly polarized wave with wavelength 10 μm and electric field strength 30 GV/m. We find that $\rho = 0.15$ μm, $v_T = 0.09$ c, $\theta = 1.2$ nr, and dE/dz = 3.3 eV / m !!! Thus this is not a very promising approach to accelerating particles to high energies.

1.5.2 Two-wave IFEL

Consider a particle acted upon by two circularly polarized waves [21]. The purpose of the second wave is to force the particle into moving in a helical trajectory. Then, if the helical motion is synchronous with the rotation of the electric field in the other wave, a net energy exchange can occur. The synchronism condition is

$$\omega_1 [\,1 - \beta_Z \cos(\theta_1)] = \omega_2 [\,1 - \beta_Z \cos(\theta_2)] \tag{1.24}$$

where the particle travels along z, ω_i is the frequency and θ_i is the angle with respect to z of the two waves. For $\theta_1 \approx 0$ and $\theta_2 \approx \pi$, we need

$$\omega_1 \approx 4\,\gamma^2\,\omega_2$$

Thus, there must be a large ratio between the frequencies of the two waves for relativistic particles.

1.5.3 Inverse synchrotron radiation

It is possible to accelerate a train of low energy electrons moving in a circle in a static transverse magnetic field, by forcing the particle orbit to cross the focal region of a laser beam [22].

1.5.4 Inverse bremsstrahlung

This technique uses a transverse static electric field to deflect the particle orbit across the path of an electromagnetic wave [23-25]. At very low energies it may offer some advantage over bending in magnetic fields.

1.5.5 Cyclotron autoresonance

In this scheme [26-35] a static longitudinal magnetic field is used to confine the particle orbit as shown in Fig. 1.8. There can be net exchange of energy if the particle motion is synchronous with a circularly polarized wave travelling in the same direction. In the case when the particle loses energy the device acts as a power source known as a cyclotron autoresonance maser (CARM). Electron acceleration up to 0.5 MeV has been achieved using microwaves as the power source. The device may be practical as a high duty factor, MeV-level injector. The helical particle orbit will limit its performance at high energies.

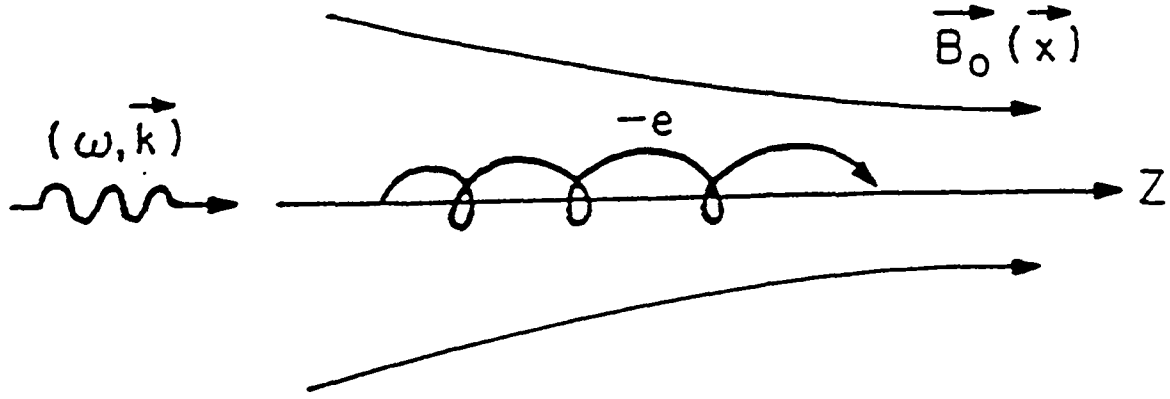

Fig. 1.8 Cyclotron autoresonance acceleration [33]

In a circularly polarized plane wave the electric field has the form

$$\begin{aligned} \mathbf{E} &= \mathbf{E}_L\,(\cos\zeta, -\sin\zeta, 0) \\ B &= \frac{\mathbf{E}_L}{c}\,(\sin\zeta, \cos\zeta, 0) \\ \zeta &= kz - \omega t + \Phi \end{aligned} \tag{1.25}$$

The equations of motion are

$$\begin{aligned} \frac{d}{dt}(\gamma\beta_X) &= \frac{e\mathbf{E}_L}{mc}(1-\beta_Z)\cos\zeta + \frac{eB_o}{m}\beta_Y \\ \frac{d}{dt}(\gamma\beta_Y) &= -\frac{e\mathbf{E}_L}{mc}(1-\beta_Z)\sin\zeta - \frac{eB_o}{m}\beta_X \\ \frac{d}{dt}(\gamma\beta_Z) &= \frac{e\mathbf{E}_L}{mc}[\beta_X\cos\zeta - \beta_Y\sin\zeta] \\ \frac{d}{dt}(\gamma) &= \frac{e\mathbf{E}_L}{mc}[\beta_X\cos\zeta - \beta_Y\sin\zeta] \end{aligned} \tag{1.26}$$

The quantity

$$\gamma\,(1-\beta_Z) = a$$

is a constant of the motion. In terms of this constant, the transverse velocity can be written

$$\beta_T^2 = \frac{2a\gamma - a^2 - 1}{\gamma^2} \tag{1.27}$$

As γ increases, β_T and d/dt ($\gamma\beta_Z$) decrease. The second constant of the motion can be written

$$\gamma(t)\left[1 - \frac{\omega_E}{\Delta\omega}\beta_T(t)\sin\alpha(t)\right] = b$$

where

$$\begin{aligned} \omega_E &= \frac{e\mathbf{E}_L}{\gamma_o mc} \\ \Delta\omega &= \frac{eB_o}{\gamma_o mc} - (1-\beta_{zo})\,\omega \end{aligned}$$

The pitch angle of the helical trajectory is defined from

$$\vec{\beta} \cdot \vec{E} = \beta_T E_L \cos\alpha \tag{1.28}$$

The particle rotates around the static field with the cyclotron frequency

$$\Omega = \frac{eB_o}{mc\gamma} \tag{1.29}$$

The net angle between the particle velocity and the electric field of the wave is

$$\phi(t) = \omega t - kz - \Omega t \tag{1.30}$$

The resonance condition, which occurs when $d\phi / dt = 0$, is

$$\Omega = \omega - k v_z \tag{1.31}$$

If the particle does not satisfy the resonance condition when it enters the static field, then p_z will be a periodic function of time, as shown in Fig. 1.9 . However, if the particle does satisfy the resonance condition initially, p_z can continue to increase until imperfections cause the resonance condition to be violated or until radiation effects become significant. This condition is known as *autoresonance*. As γ increases the cyclotron frequency decreases, but the Doppler shifted wave seen in the particle frame decreases by the same factor.

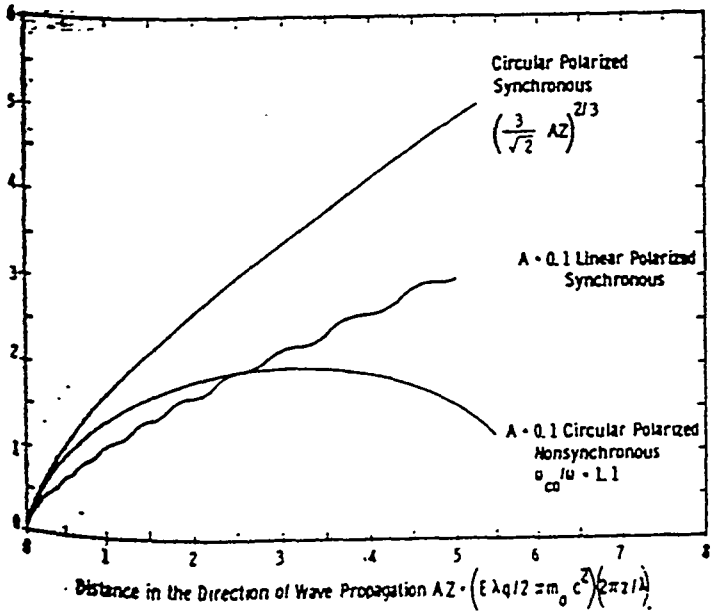

Fig. 1.9 Energy of particle as a function of distance through the acceleration region [28].

The distance along z that the particle travels during one cyclotron period is

$$z_P = \frac{2\pi m\gamma}{eB_o}\beta_z c$$

while the distance the wave travels during this same time is

$$z_W = \frac{2\pi m\gamma}{eB_o}c$$

The difference in distances along z is

$$\Delta z = \frac{2\pi mc\gamma}{eB_o}(1-\beta_z) \tag{1.32}$$

If we impose the resonance condition, we find that $\Delta z = \lambda$, as expected for a second order acceleration process.

Scaling arguments [28] show that the energy gain in cyclotron autoresonance acceleration goes like

$$\Delta E = mc^2\left\{\frac{3}{\sqrt{2}}\alpha Z\right\}^{\frac{2}{3}} \tag{1.33}$$

where α is the dimensionless field strength parameter and

$$Z = \frac{2\pi z}{\lambda}$$

is the dimensionless length. For comparison a conventional linac scales like

$$\Delta E = mc^2\alpha Z \tag{1.34}$$

The cyclotron mechanism is more efficient up to several MeV energy.

A cyclotron resonance accelerator has been proposed [33] using 20 MW of 11.4 GHz microwaves as the power source. The magnetic field is tapered from 0.24 to 0.70 T to keep the orbit radius from increasing. The expected energy gain is 2.3 MeV.

1.6 Limited interaction in vacuum with no static fields

A number of acceleration schemes have been proposed for accelerating particles in vacuum with no static fields [36-42]. These schemes involve sending the particle on a straight path through the focal region of a laser beam. Then, if the region of interaction could be somehow limited, a net acceleration might occur. If the particle and the wave travel in the same direction, their velocity difference is

$$\Delta v = (1 - \beta) c$$

The maximum useful interaction length is the distance over which the particle slips behind the wave by $\lambda / 2$. Beyond this the particle begins to see fields of the opposite polarity and decelerates. The *slip time* is given by

$$t_{slip}\, \Delta v = \frac{\lambda}{2}$$

Then we can define the *slip distance* as

$$L_{slip} = c\, t_{slip} \propto \lambda \gamma^2 \tag{1.35}$$

Nonrelativistic beams can be accelerated in passing through a laser focus, although most particles also receive large deflections. Realistic models of the focal region fields as described in Sec. 1.3 predict smaller accelerations than simple plane wave models.

One proposal [38] for limited the interaction region involves having the particle trajectory cross the laser focus at an angle, as shown in Fig. 1.10.

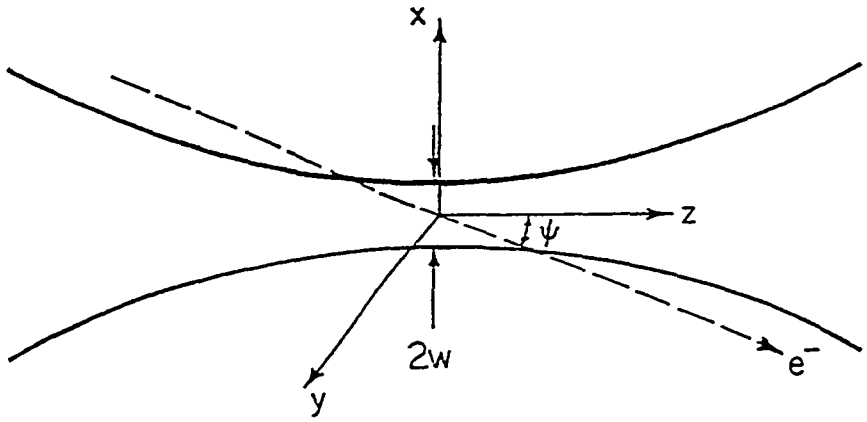

Fig. 1.10 A limited interaction region? [2]

The idea is to arrange the path length of the particle through the focus to be less than the slip distance. Another scheme [42] uses axicon focus cells identical to those used for inverse Cerenkov acceleration, but without the phase matching gas present. Acceleration of about 12 MeV is predicted for 10^{13} W of CO_2 laser power.

Palmer [9] has raised a number of arguments questioning the possibility of acceleration in vacuum solely due to far fields. He states his conclusions in the form of a theorem:

> No combination of far fields, in an otherwise field-free vacuum, can produce first-order net acceleration.

By "otherwise field-free" he means that no static fields are present and that a second incoming electromagnetic wave is not used to wiggle the particle trajectory. By "first order" he means he is only considering cases where the energy exchange is proportional to the first power of the accelerating field. By "net acceleration" he means that you must consider the total effects involved in getting the particle from one field free region to another.
The essence of one of his proofs is:

1. Real photons cannot interact with particles in a vacuum because of energy-momentum conservation.

2. Far fields consist of real (on mass shell) photons.

3. Therefore, far fields cannot accelerate particles in a vacuum.

A second, classical proof uses the facts that a single plane wave cannot give net acceleration and that far fields are made up of sums of plane waves.

The counter argument has been made that the uncertainty principle allows far field interactions to violate energy-momentum conservation by ΔE, provided that the interaction time is limited to

$$\Delta t \leq \frac{h}{\Delta E}$$

One must be careful in considering the limited interaction region to integrate the interaction from $-\infty$ to $+\infty$ and to take into account curvature in the wavefronts. If the interaction is limited by physical obstructions, such as thin windows or holes in mirrors, field sources on the boundaries must also be considered.

Chapter 2 Inverse Cerenkov Acceleration

2.1 General considerations

We saw in the previous chapter that a particle can remain synchronously in phase with an electromagnetic wave in a dielectric, if the particle and wavevector cross at an angle given by

$$\cos\theta = \frac{1}{\beta n} \tag{2.1}$$

where βc is the particle velocity and n is the index of refraction for the dielectric medium. The particle trajectory is a straight line. Only one incident wave is required, although it is most efficient if the wave is focused in a cone onto the particle axis. The major difficulties with the method are multiple scattering and electrical breakdown of the medium. This type of accelerator would be most useful at high energies, where scattering effects become less important [43-49].

The most important features of the inverse Cerenkov fields can be derived from a simple two plane wave model. Consider two waves crossing the particle axis at the angle θ, as shown in Fig. 2.1. The wavevector in the dielectric is

$$k' = \frac{2\pi}{\lambda'} = \frac{2\pi n}{\lambda} = nk \tag{2.2}$$

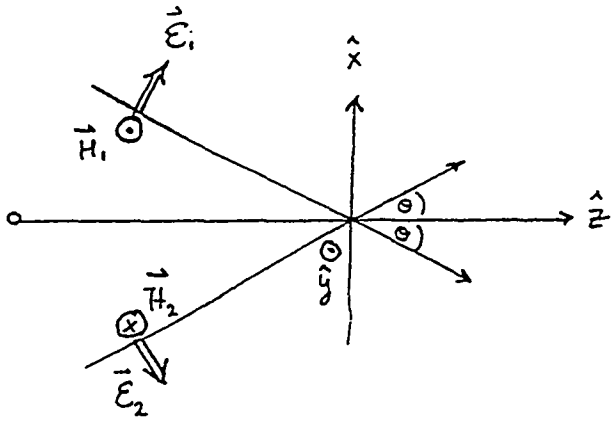

Fig. 2.1 Two plane wave model of inverse Cerenkov interaction.

By addition of the two waves we find that

$$\begin{aligned} E_X &= E_o \cos\theta \left\{ e^{i[k'(-x\sin\theta + z\cos\theta) - \omega t]} - e^{i[k'(x\sin\theta + z\cos\theta) - \omega t]} \right\} \\ &= -2i E_o \cos\theta \sin(n k x \sin\theta) \exp(i n k z \cos\theta - i \omega t) \end{aligned} \tag{2.3}$$

Similarly, we find that

$$\begin{aligned} E_Z &= 2 E_o \sin\theta \cos(n k x \sin\theta) \exp(i n k z \cos\theta - i \omega t) \\ H_Y &= -2i \frac{E_o}{Z_o} n \sin(n k x \sin\theta) \exp(i n k z \cos\theta - i \omega t) \end{aligned} \tag{2.4}$$

We see that the solutions have the form of standing wave in the transverse plane multiplied by a travelling wave along z. The two transverse fields are 90° out of phase with respect to E_Z. The accelerating field E_Z is proportional to $E_o \sin\theta$. The magnetic field is enhanced by a factor n relative to fields in vacuum.

The phase velocity is

$$v_{ph} = \frac{\omega}{k_Z'} = \frac{\omega}{n k \cos\theta} = \beta c \tag{2.5}$$

In the quantum picture ICA is possible because the dielectric spreads out the light cone so that it intersects the parabolic energy-momentum surface of the particle in two locations.

Because of the scattering in the dielectric, a practical ICA uses gas as the dielectric medium. Then for relativistic particles we have

$$\begin{aligned} n - 1 &\approx 10^{-4} \\ \beta &\approx 1 \end{aligned}$$

and the Cerenkov relation requires that $\theta << 1$. In this limit the synchronism relation can be written

$$2(n-1) \approx \theta^2 + \frac{1}{\gamma^2} \tag{2.6}$$

The index of refraction can be changed by changing the gas pressure P according to

$$n - 1 = (n_o - 1) \frac{P}{P_o} \tag{2.7}$$

where the subscript o refers to quantities at atmospheric pressure. For example, hydrogen

gas has n_o - 1 = 1.38 10^{-4}. At 1.8 atm and 50 MeV electron energy, the Cerenkov angle is 20 mr.

2.2 Problems with acceleration in a medium

The dielectric medium introduces energy loss, the possibility for electrical breakdown, and scattering. Energy loss due to ionization is proportional to the density of the material. In a gas under typical pressures this is ~ 10^{-4} times solid densities, so the energy loss for minimum ionizing particles should be ~ 0.2 keV / cm. The energy loss of electrons due to bremsstrahlung exceeds the ionization loss for hydrogen above 800 MeV, but is also proportional to the density of the material.

Electrical breakdown of the gas has the potential to produce free charges and disrupt the desired field pattern. It also affects the optical properties by locally modifying the index of refraction. Breakdown is a complicated problem dependent on the type of gas, purity, and pressure, and on the wavelength, pulse length, and repetition rate of the laser. It is desirable for the gas to have a high ionization potential. It is desirable for the laser to have a long wavelength (less energetic photons). The relevant pulse length regime is for *ps* pulses, where unfortunately, few breakdown measurements have been made.

Gas breakdown is believed to begin either through tunneling or multiphoton ionization. Once any free charge has been produced, an avalanche can result when the electron accelerates in the field, collides with other gas molecules, produces more electrons, etc. It is known from the STI experiment at BNL that the threshold for breakdown for 220 ps CO_2 light pulses in H_2 at 1.8 atm is greater than 0.5 TW / cm^2.

Multiple scattering changes the distribution of electron position and angle. This is detrimental because it causes the beam emittance to increase and because it can change a particle's phase with respect to the wave and causes particles to get out of synchronism. In the gaussian approximation the r.m.s: width is given by the Highland formula

$$\theta_{ms} = \frac{13.6\,MeV}{\beta pc} z_1 \sqrt{\frac{L}{L_R}} \left[1 + 0.038 \ln\left(\frac{L}{L_R}\right)\right] \tag{2.8}$$

which is accurate to around 10%. The radiation length of hydrogen is 7 km at 1 atm. Since the size of this effect scales like 1 / p it is advantageous to use ICA at high energies. The r.m.s. transverse size of the beam increases as

$$y_{rms} = \frac{1}{\sqrt{3}} L\,\theta_{ms} \tag{2.9}$$

2.3 Stanford University experiments

The first positive demonstration of ICA [50-53] was performed at Stanford U. around 1980. In these experiments a 1.06 μm wavelength, linearly polarized beam from a 30 MW YAG laser was used. The laser crossed the path of a 102 MeV electron beam at the Cerenkov angle. The interaction took place in a cell containing hydrogen gas. The electron momentum was measured after the interaction region with a dipole magnet spectrometer.

The experiment observed a modulation of the energy spectrum. By changing the gas pressure, it was shown that the energy exchange had the correct dependence on the value of n. Additional checks were made by changing the gas to methane and changing the velocity of the electron beam. The observed energy shift was ~ 50 keV. With a 7 cm interaction length, this corresponds to an energy gradient of ~ 7 keV / cm.

A separate experiment studied multiple scattering as a function of pressure in the gas cell [54]. The growth in beam radius was measured using phosphor coated screens and Cerenkov radiators after the gas cell. The measured beam size agreed well with the predictions from the Highland formula.

2.4 Axicon field geometry

A much more practical and efficient field distribution [46,55] to use for ICA comes from using a radially polarized, axicon focused laser beam, as shown in Fig. 2.2. We will first present a simple derivation for the fields present in the axicon focus. Consider in Fig. 2.3 an infinite number of plane waves all converging on the particle axis at the Cerenkov angle and uniformly distributed in azimuthal angle. Then the main contribution to dE_Z from each one of the waves is

$$dE_Z = E_o \sin\theta \, e^{-i\Psi} \frac{d\phi}{2\pi} \tag{2.10}$$

and where the phase factor is

$$\Psi = n k x \sin\theta \cos\phi + n k y \sin\theta \sin\phi - n k z \cos\theta + \omega t \tag{2.11}$$

If we let (x,y,z) correspond to the field observation point, then

$$E_Z(x,y,z) = \frac{E_o}{2\pi} \sin\theta \, e^{i n k z \cos\theta - i\omega t} \; I(\phi) \tag{2.12}$$

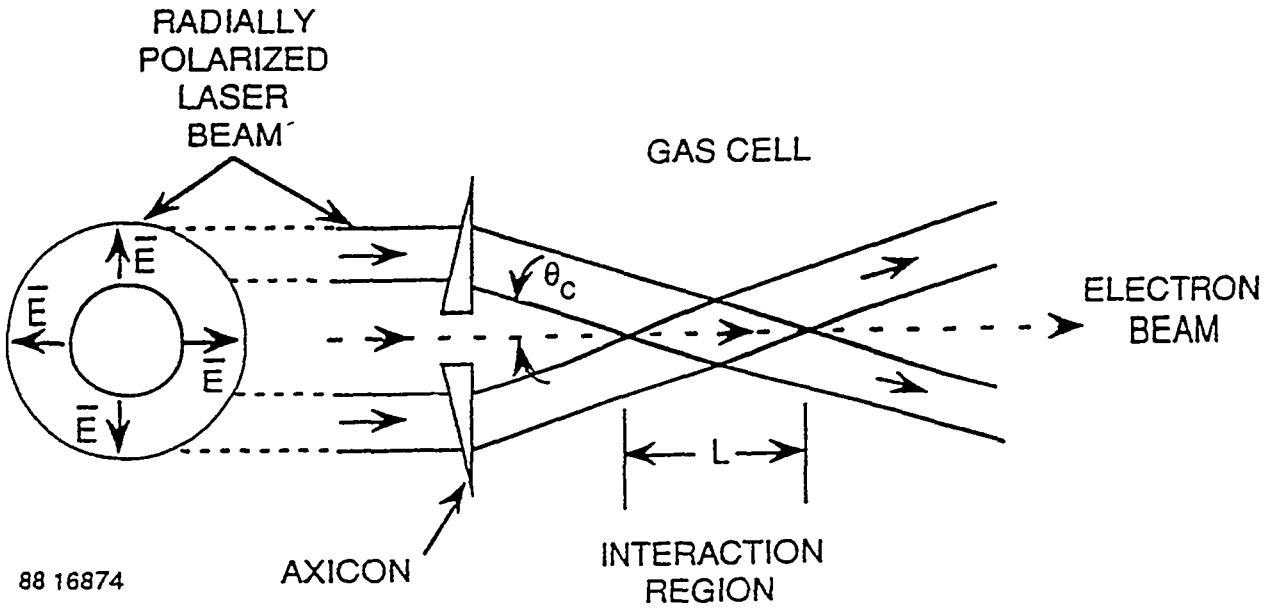

Fig. 2.2 Axicon geometry for inverse Cerenkov acceleration [55].

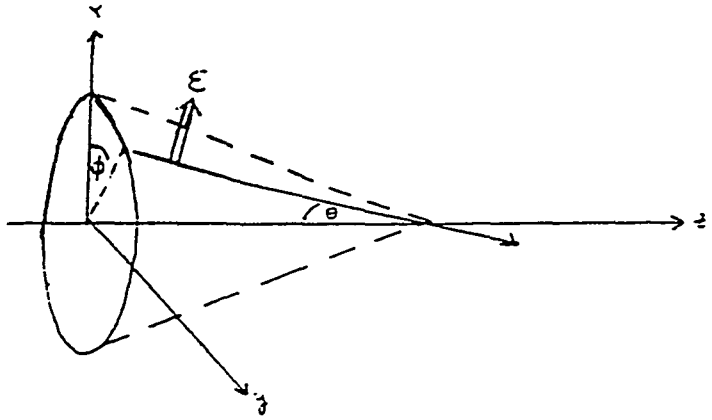

Fig. 2.3 An infinite number of plane wave sections converging on the particle trajectory at the Cerenkov angle.

where the integral I is given by

$$I(\phi) = \int_0^{2\pi} e^{-ikn\sin\theta\,(x\cos\phi + y\sin\phi)}\, d\phi \tag{2.13}$$

If we now use the Bessel function relation,

$$\int_0^{2\pi} e^{iA\cos\phi + iB\sin\phi}\, d\phi = 2\pi J_o(\sqrt{A^2 + B^2}) \tag{2.14}$$

then we can write

$$E_Z(r,z) = E_o \sin\theta\, J_o(nkr\sin\theta)\, e^{inkz\cos\theta - i\omega t} \tag{2.15}$$

From symmetry E_ϕ , B_R , and B_Z are zero. From div E = 0, we find that

$$E_R(r,z) = -iE_o \cos\theta\, J_1(nkr\sin\theta)\, e^{inkz\cos\theta - i\omega t} \tag{2.16}$$

while from the $(\text{curl } E)_\phi$ Maxwell equation, we find

$$B_\phi(r,z) = -i\frac{E_o}{c}\, n\, J_1(nkr\sin\theta)\, e^{inkz\cos\theta - i\omega t} \tag{2.17}$$

Note that the transverse components have a J_1 radial dependence, so they vanish on the axis. The transverse components are also 90° out of phase from the longitudinal (accelerating) component. The magnetic field is proportional to n .

The equations of motion in the axicon field are

$$\begin{aligned} \frac{d}{dt}p_\phi &= 0 \\ \frac{d}{dt}p_Z &= eE_Z \\ \frac{d}{dt}p_R &= e(E_R - \beta c B_\phi) \end{aligned} \tag{2.18}$$

If we make use of the relation

$$B_\phi = \frac{n}{c\cos\theta}E_R = \beta n^2 \frac{E_R}{c} \tag{2.19}$$

we can rewrite the radial equation of motion as

$$\frac{d}{dt}p_R = e\,E_R(1 - \beta^2 n^2) \tag{2.20}$$

This shows clearly that the transverse force on a particle does not vanish in the limit $\beta \rightarrow 1$, as it does for acceleration in vacuum. Note that the net radial force is directed oppositely to E_R. Because of the phase difference between the longitudinal and transverse forces, particles in 1/4 of possible phases accelerate and focus simultaneously, as shown in Fig. 2.4..

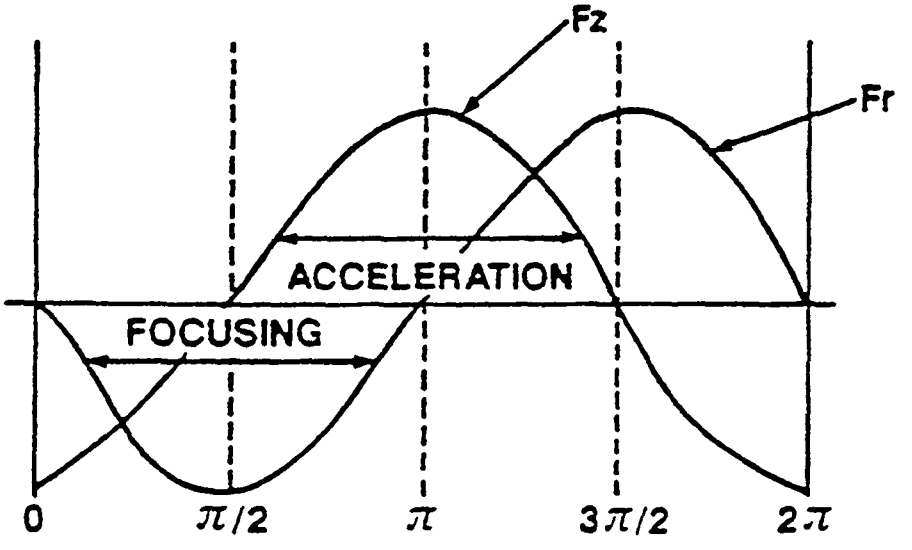

Fig. 2.4 Longitudinal and radial forces in ICA as a function of the particle-wave phase [55].

The maximum useful beam radius is constrained by the location of the first zero of the J_o Bessel function

$$n\,k\,r_B \sin\theta < 2.40$$

$$\theta\,\frac{r_B}{\lambda} < 0.38$$

This gives $r_B \sim 200$ μm for a CO_2 laser in hydrogen at 1.8 atm.

The peak field location is determined by the first maximum of the J_1 Bessel function

$$n k r_P \sin\theta = 1.8$$

$$\theta \frac{r_P}{\lambda} = 0.29$$

This gives $r_P \sim 150$ μm for the same conditions mentioned above. Since the peak field location is the place that is most likely to break down, we want to keep $r_B < r_P$. Since we have $J_1(1.8) = 0.58$, $E_P \sim 0.58\, E_o$.

An axicon acceleration cell has a "dead" space between the axicon mirror and the interaction region of

$$D = \frac{R_1}{\tan\theta} \tag{2.21}$$

where R_1 is the inner radius of the axicon lens. The energy gain in the cell is [46]

$$\Delta E = 69 \sin\theta \sqrt{\frac{PL}{\lambda}} \cos\Phi \tag{2.22}$$

where P is the laser power, L is the interaction length, λ is the laser wavelength, and Φ is the phase.

For certain phase regions the axicon transverse focusing force is quite effective in restraining the beam emittance growth due to multiple scattering. The focusing fields produce an equivalent betatron focusing parameter given by

$$\beta_\perp^2 = \frac{\gamma m c^2 \lambda}{\pi e E_o \theta^2 \sin\Phi} \tag{2.23}$$

2.5 Acceleration experiment at BNL

An experimental program [56-57,97] is currently underway at the Accelerator Test Facility (ATF) [58-67] at BNL to study the ICA process with a radially polarized, axicon focused CO_2 laser beam. One data run [68] took place in 1994 and a second is scheduled for 1995. The test beam for the first run was a 40 MeV electron beam produced in the ATF photocathode rf gun. Hydrogen gas was used as the phase matching medium.

The radial polarization is made from the linearly polarized output of the CO_2 laser in a double interferometer [69-71]. The beam is split and each half passes through spiral phase delay plates of opposite handedness, as shown in Fig. 2.5. The spiral phase delay plate is made by depositing a ZnSe coating on a circular ZnSe substrate. The coating thickness is made proportional to the azimuthal angle up to a maximum thickness of λ . Two beams are produced with azimuthal intensity dependences of $I_o \cos^2 \theta$ and $I_o \sin^2 \theta$ respectively. After these beams are recombined, the final beam intensity is independent of azimuthal angle.

The laser had a power of 580 MW and a pulse duration of 220 ps for the 1994 run . The gas cell, shown in Fig. 2.6, had 2.1 μm thick diamond film windows to minimize multiple scattering. The total electron path in the gas cell was 43 cm, while the interaction length was ~12 cm. The Cerenkov angle for the gas was 20 mr.

The change in electron momentum was measured using an spectrometer consisting of a dipole magnet, three quadrupole magnets, and phosphor screen viewed by an image intensifier and TV camera. The measured energy spectrum with the laser off and on is shown in Fig. 2.7. The measured data agree fairly well with model predictions. The data for the high energy gain end of the spectrum is shown in Fig. 2.8. The maximum energy gain was ~3.7 MeV, corresponding to an energy gradient of ~ 30 MeV / m. The observed signal as a function of gas pressure is shown in Fig. 2.9. This data confirmed that the maximum acceleration occurred when the Cerenkov relation was satisfied.

The acceleration achieved during the 1994 run was limited by the amount of laser power in the gas cell. This in turn was limited by optical damage to the input lens of the axicon telescope. For the next run the laser optics has been adjusted to allow the full 5 GW of available power to be delivered to the experiment. The interaction length is expected to increase to ~20 cm. Taken together 12 MeV acceleration and 60 MeV / m gradient are the goals for the next run.

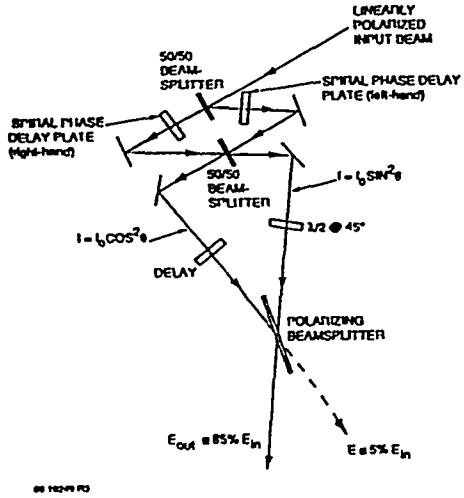

Fig. 2.5 Principle for producing radially polarized laser beam [71].

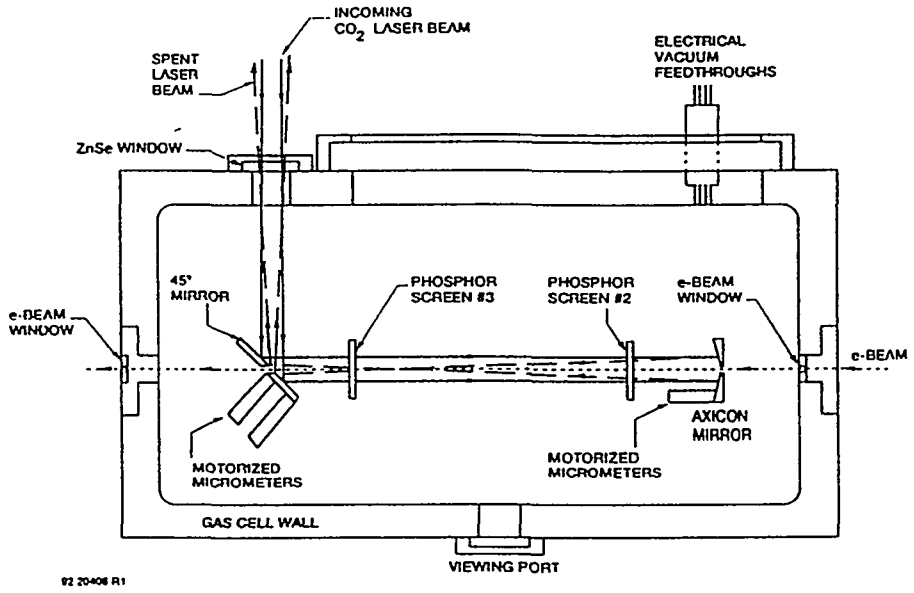

Fig. 2.6 Schematic plan view of ICA gas cell [68].

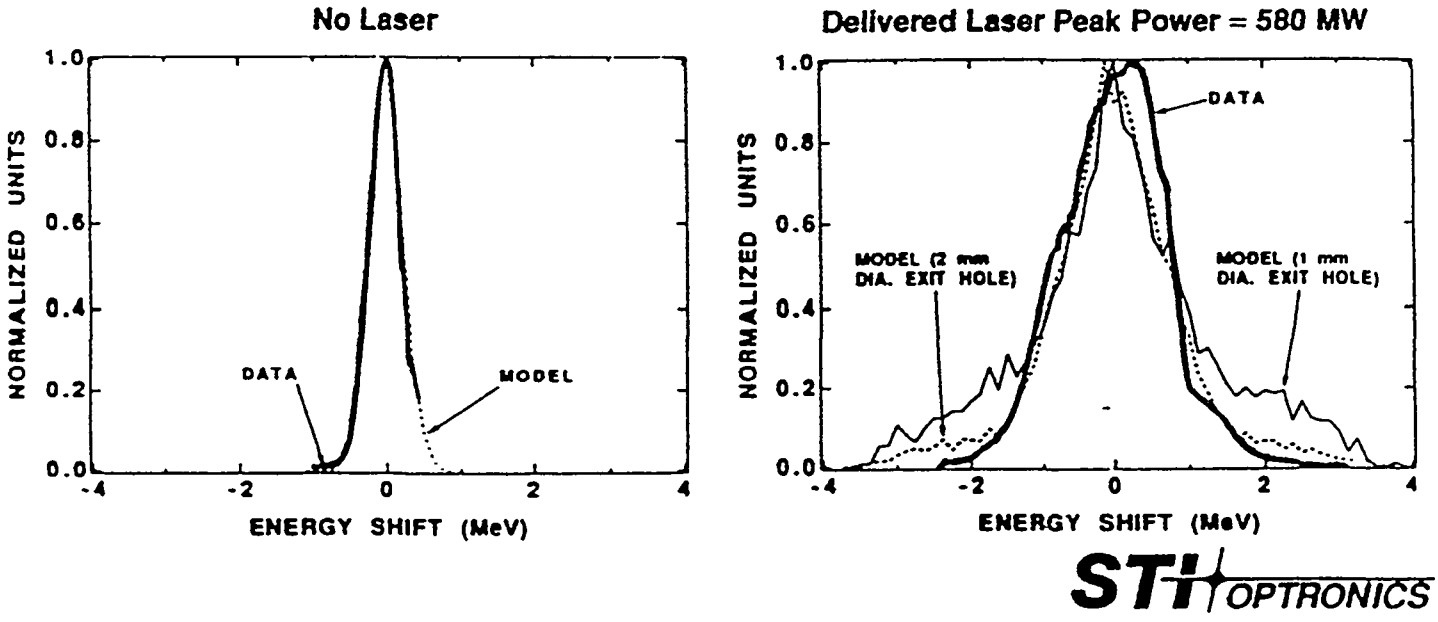

Fig. 2.7 Energy modulation spectrum for ICA interaction [68].

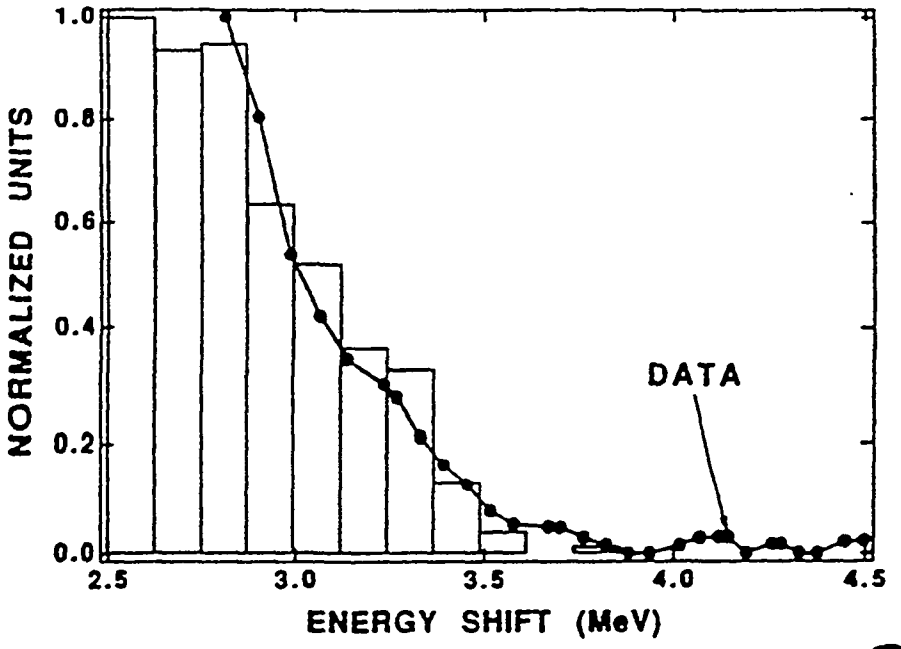

STI OPTRONICS

Fig. 2.8 Data for high energy gain tail of energy modulation spectrum [68].

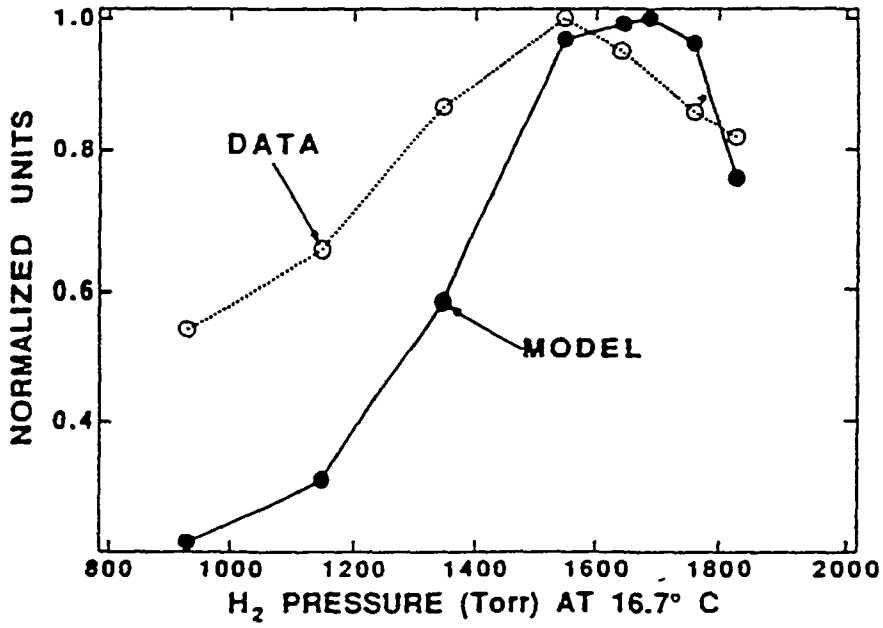

Fig. 2.9 Observed signal as a function of pressure in the hydrogen gas cell [68].

2.6 Future directions

One area of research for improving the ICA process is the investigation of new gas mixtures that may posses resonances in the frequency range covered by high power laser sources [91]. Many molecules have natural oscillation frequencies where the index of refraction has a large increase in magnitude. Using such a gas, the n value needed for phase synchronization could be achieved at a lower gas pressure than would otherwise be necessary. This would give a given amount of acceleration with less multiple scattering and emittance growth. The use of a Ti-sapphire laser with Li vapor at a pressure of 0.01 atm is one possibility, which might give acceleration gradients greater than 5 GeV / m.

A 100 MeV energy gain demonstration experiment has been proposed [92-93] for the ATF. The proposed experiment would prebunch the 65 MeV input beam in a short ICA cell, let the beam drift (possibly using a magnetic compressor stage), and then let the beam interact with several stages of acceleration cells. Staging would be done by reflecting the spent axicon beam from one cell off the inner surface of a hollow cylindrical optical guide, as shown in Fig. 2.10. The necessary CO_2 laser power is ~200 GW.

Studies have also been made of using the inverse Cerenkov interaction in a focusing lens [94-95].

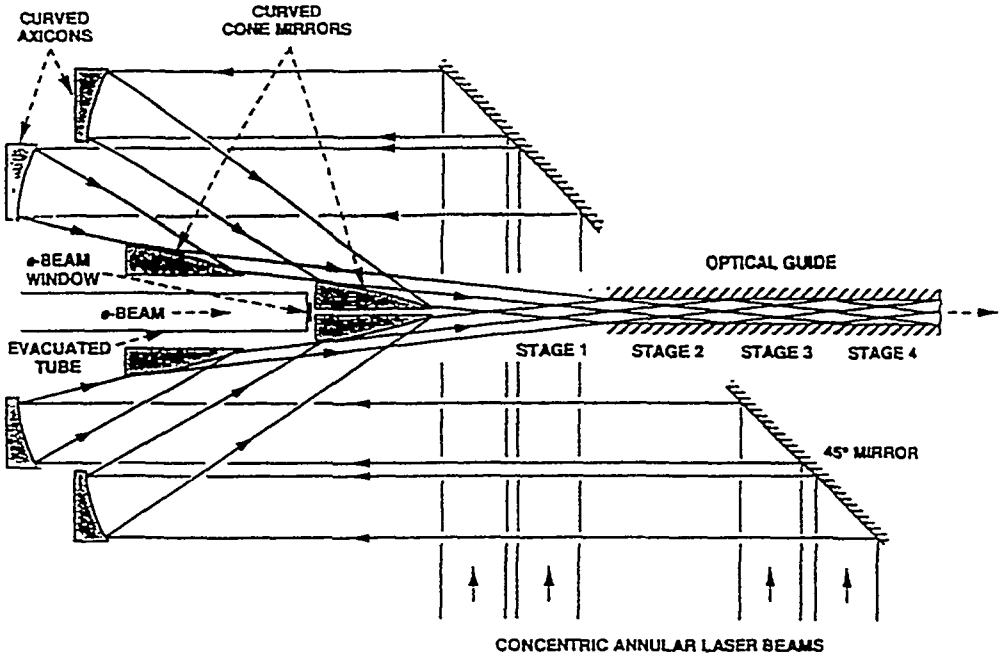

Fig. 2.10 Optical configuration for a 4-stage axicon focused ICA.

Chapter 3 IFEL acceleration using static magnetic wigglers

3.1 General considerations

In the inverse free electron laser (IFEL) accelerator concept [72-77] the particle beam is made to wiggle back and forth through the laser beam using a series of alternating dipole fields, as illustrated in Fig. 3.1. The physics of the interaction has been demonstrated in many experiments on the production of FEL radiation. This scheme should be capable of accelerating electrons up to several hundred GeV with gradients of several hundred MeV / m. Since it is a second order process, both e^+ and e^- can be accelerated with the same laser phase, which could be important in reducing space-charge effects. The production of synchrotron radiation and attenuation of the laser power limit the maximum energy gradient.

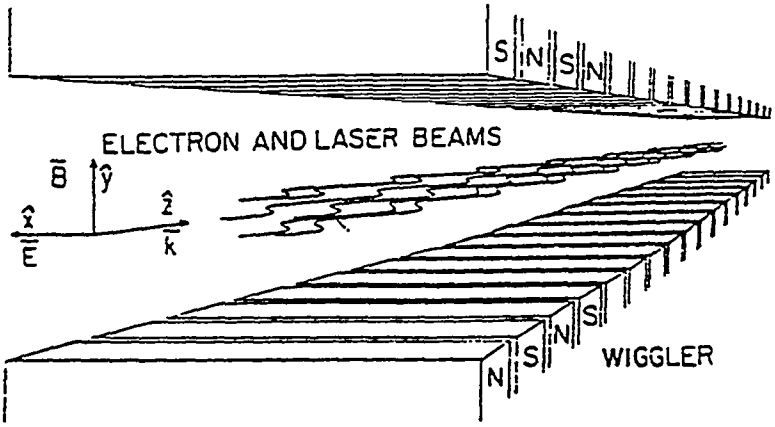

Fig. 3.1 Schematic diagram illustrating IFEL accelerator [76].

The basic principle [7] of the acceleration mechanism is illustrated in Fig. 3.2, which shows the electric and magnetic forces acting on the particle at a given instance of time.

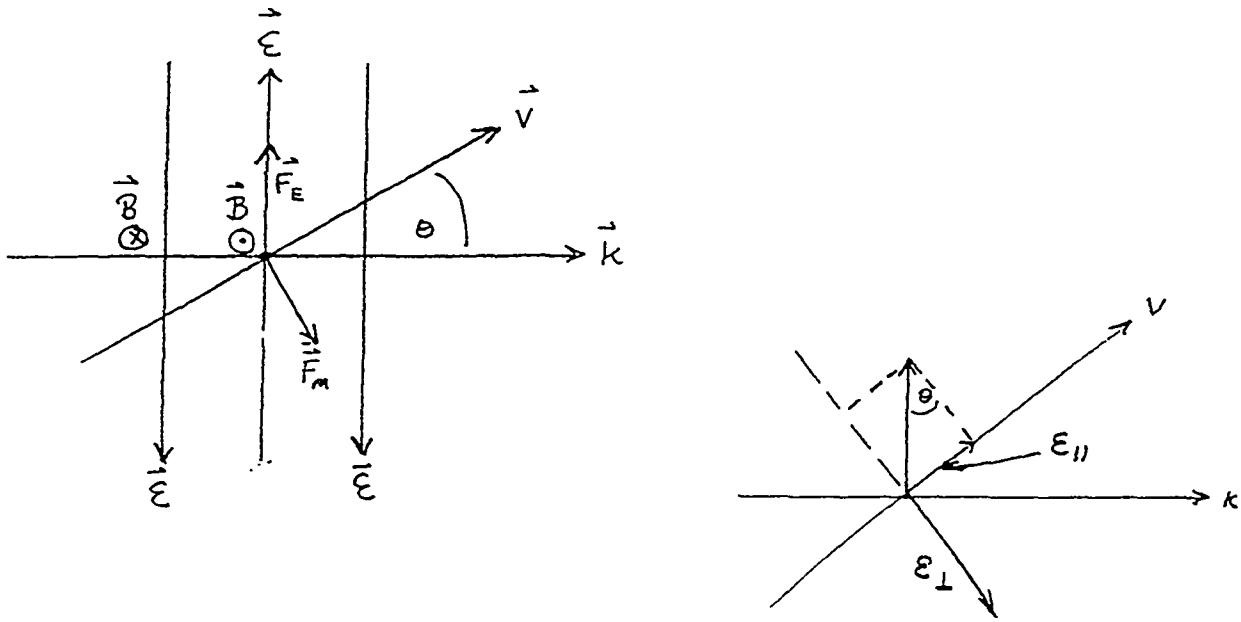

Fig. 3.2 Interaction of a particle with transverse velocity component and an electromagnetic wave.

The net fields seen by the particle are

$$\begin{aligned} E_L &= E_o \sin\theta \simeq E_o \theta \\ E_\perp &= E_o (\cos\theta - \beta) \simeq 0 \end{aligned} \tag{3.1}$$

There will be a small acceleration proportional to $E_o\,\theta$. However, if nothing else is done, the particle and wave will slip out of phase and no net acceleration will result. At any distance z the particle sees the field

$$\begin{aligned} E(z) &= E_o \exp\left[ikz\left(1 - \frac{1}{\beta\cos\theta}\right)\right] \\ &= E_o\, e^{ik_W z} \end{aligned} \tag{3.2}$$

In the limit of high energy and small angle θ , the synchronism condition becomes

$$k_w \simeq k\left(\frac{\theta^2}{2} + \frac{1}{2\gamma^2}\right) \tag{3.3}$$

For very high energies, where $\theta^2 >> 1/\gamma^2$,

$$k_w \simeq \frac{\pi\,\theta^2}{\lambda} \tag{3.4}$$

During the one half slip-period when the particle is accelerating, the energy gain is

$$\begin{aligned} \Delta E &\simeq e E_o \theta \int \cos(k_w z)\, dz \\ &\simeq \frac{2 e E_o \lambda}{\pi\,\theta} \end{aligned} \tag{3.5}$$

In the IFEL the direction of the magnetic field is reversed at this point, changing the direction of the particle's transverse motion, and allowing the particle to continue gaining the same amount of energy in the second half slip-period. This process is continued over many periods, allowing a substantial overall energy gain to occur.

An alternative viewpoint is to consider the static wiggler magnetic field as a travelling electromagnetic wave in the electron rest frame [74]. This wiggler wave then interferes with the incident laser wave forming a pondermotive beat wave, which traps and accelerates particle bunches.

Beginning with the second order synchronism condition given in Eq. 1.8, it is possible to write the IFEL synchronism condition for the high energy, small angle limit as

$$\lambda = \frac{\lambda_w}{2\gamma^2}(1 + K^2) \tag{3.6}$$

where $K^2 \simeq \theta_R{}^2 \gamma^2$ is a dimensionless parameter and θ_R is the typical absorption angle of the radiation. It is also possible to write the synchronism condition in the form

$$\beta c = \frac{\omega}{k + k_w} \tag{3.7}$$

where we see that the wiggler acts to contribute an extra "momentum" k_W .

It is possible to change the synchronism condition by using a gas inside the wiggler, instead of vacuum.

$$\lambda_w \propto \frac{2\lambda}{\alpha^2 - \theta_C^2} \tag{3.8}$$

where θ_C is the Cerenkov angle. The parameter

$$\alpha = \frac{e B_w \lambda_w}{2\pi p}$$

where p is the particle momentum. The energy gradient is proportional to $E_o\,\alpha$, so we want a large value of α. The gas makes it possible to get synchronism with a lower wiggler field, thereby reducing the synchrotron radiation losses. Of course, the gas also introduces the problems of scattering discussed in the previous chapter.

Besides the planar type of wiggler discussed to now, it is also possible to use a helical wiggler, where the dipole field rotates as a function of z. Such a field can be produced by using two helical current windings with the current flowing in opposite directions.

The pitch angle θ can be determined from

$$\begin{aligned} \cos\theta &= \frac{v_z}{v_s} \\ &= \frac{1}{\sqrt{1+\alpha^2}} \end{aligned} \tag{3.9}$$

where v_s is the rate of change along the arc of the helical path. In terms of the helical wiggler geometry

$$\theta \propto \alpha = \frac{2\pi R_w}{\Lambda_w} \tag{3.10}$$

where R_W is the radius of the wiggler. From the radial equation of motion, we have

$$m c \beta_T \gamma = e v_z B_w \tau = e B_w \Lambda_w$$

where τ is the time to go through one period of the wiggler. It follows that

$$\beta_T = \frac{e B_w \Lambda_w}{m c \gamma}$$

Thus, in terms of the particle dynamics we have

$$\theta \sim \alpha = \frac{e B_w \Lambda_w}{p_Z} \tag{3.11}$$

Now assume that a circularly polarized laser beam is travelling down the axis of the helical wiggler.

$$\begin{aligned} \vec{E} &= \vec{E}_X + i\vec{E}_Y \\ &= \vec{E}_o \exp[ik(z - ct) + \Phi_o] \end{aligned} \tag{3.12}$$

The z position of the particle is

$$z = \beta c t \cos\theta$$

Thus the electric field seen by the particle at position z is

$$\vec{E} = \vec{E}_o \exp\left[ikz\left(1 - \frac{1}{\beta\cos\theta}\right) + \Phi_o\right] \tag{3.13}$$

The relative phase between E and the particle motion along the helix is then

$$\Phi = k\left(1 - \frac{1}{\beta\cos\theta}\right) - k_w \tag{3.14}$$

Thus, the particle in a helical wiggler can see a constant component of E acting along it's motion if $\Phi = 0$ or

$$k_w = k\left(\frac{1}{\beta\cos\theta} - 1\right) \tag{3.15}$$

This is not the case for a planar wiggler. A particle there always sees the same sign of force, but its magnitude varies. The accelerating efficiency is thus smaller for the planar wiggler, although most wigglers have used the planar configuration for simplicity of construction.

3.2 Accelerator equations (CPZ analysis)

Courant, Pellegrini and Zakowicz (CPZ) analyzed the IFEL equations of motion [76-77] in the relativistic limit where $\beta_T << \beta_Z \approx 1$. They also assumed low density beams and neglected any attenuation of the laser power as a function of z.

The transverse canonical momentum can be written

$$\vec{p}_T = m\gamma\vec{v}_T + e(\vec{A}_L + \vec{A}_w) \tag{3.16}$$

where A is the vector potential and a small contribution due to radiation reaction is ignored. The longitudinal dynamics must include the effects of synchrotron radiation

$$mc^2\frac{d\gamma}{dt} = e\vec{v}_T\cdot\vec{\mathrm{E}}_L - P_{rad} \tag{3.17}$$

where the subscript L refers to the laser and the radiated power is given by

$$P_{rad} = \frac{2}{3}\frac{e^2}{c}\gamma^6[\dot{\beta}^2 - (\vec{\beta}\times\dot{\beta})^2] \tag{3.18}$$

in gaussian units. The magnetic field of the helical wiggler can be written

$$\vec{\mathrm{B}}_w = (B_w\cos(k_w z), B_w\sin(k_w z), 0) \tag{3.19}$$

where

$$k_w = \frac{2\pi}{\Lambda_w} \tag{3.20}$$

and Λ_w is the wiggler period.We note that this is only an approximation to the true wiggler field since it neglects the longitudinal component and variations of the fields in x and y required by Maxwell's equations. The electric field of the laser is

$$\begin{aligned}\vec{\mathrm{E}}_L &= (\mathrm{E}_o\sin(\xi), \mathrm{E}_o\cos(\xi), 0)\\ \xi &= kz - \omega t\end{aligned} \tag{3.21}$$

The strength of the wiggler and laser fields are written in terms of the dimensionless parameters

$$\begin{aligned}K &= \frac{eB_w\Lambda_w}{2\pi mc} = 93.4\,B_w[T]\,\Lambda_w[m]\\ K_L &= \frac{e\mathrm{E}_o\lambda}{2\pi mc^2}\end{aligned} \tag{3.22}$$

For typical values of $B_W = 1$ T, $\Lambda_W = 1$ cm, $E_o = 10$ GV / m, and $\lambda = 10$ μm, $K \approx 30\,K_L$ and thus terms proportional to K_L may often be neglected.

For $K << \gamma$ the transverse components of the particle velocity can be written

$$\begin{aligned} v_X &= c\frac{K}{\gamma}\cos(k_w z) + c\frac{K_L}{\gamma}\cos\xi \\ v_Y &= c\frac{K}{\gamma}\sin(k_w z) - c\frac{K_L}{\gamma}\sin\xi \end{aligned} \tag{3.23}$$

The z component can be written

$$\frac{v_Z}{c} = 1 - \frac{1 + K^2 + K_L^2 + 2KK_L\cos\psi}{2\gamma^2} \tag{3.24}$$

where the phase factor is

$$\psi = (k + k_w)z - \omega t \tag{3.25}$$

Finally the accelerator equations describe how the energy γ and the phase ψ change with z.

$$\begin{aligned} \frac{d\gamma}{dz} &= A\frac{K}{\gamma}\sin\psi - \frac{2}{3}r_e k_w^2\gamma^2(K^2 + K_L^2 + 2KK_L\cos\psi) \\ \frac{d\psi}{dz} &= k_w - k\left(\frac{1 + K^2 + K_L^2 + 2KK_L\cos\psi}{2\gamma^2}\right) \end{aligned} \tag{3.26}$$

where

$$A = \frac{e\,E_o}{m\,c^2}$$

A similar analysis for the planar wiggler has the solution

$$\begin{aligned} \frac{d\gamma}{dz} &= \frac{A}{2}\frac{K}{\gamma}[J_o(G) - J_1(G)]\sin\psi - \frac{1}{3}r_e k_w^2\gamma^2\left(K^2 + K_L^2 + 2KK_L[J_o(G) + J_1(G)]\cos\psi\right) \\ \frac{d\psi}{dz} &= k_w - \frac{k}{2\gamma^2}\left(1 + \frac{K^2}{2} + \frac{K_L^2}{2} + KK_L[J_o(G) - J_1(G)]\cos\psi\right) \end{aligned}$$

where J_0 and J_1 are Bessel functions and

$$G = \frac{kK^2}{8k_w\gamma^2}$$

After imposing the resonance condition, Eq. 3.15, only one of the functions K(z) or k_w (z) may be arbitrarily specified. Three cases have been considered:

1. constant wiggler period
2. constant wiggler magnetic field strength
3. constant wiggler strength parameter K

Fig. 3.3 shows how the energy varies with distance in a constant period accelerator. The energy quickly reaches saturation due to radiation losses that are proportional to γ^4. Small periods give the maximum initial acceleration rate, but they also saturate faster.

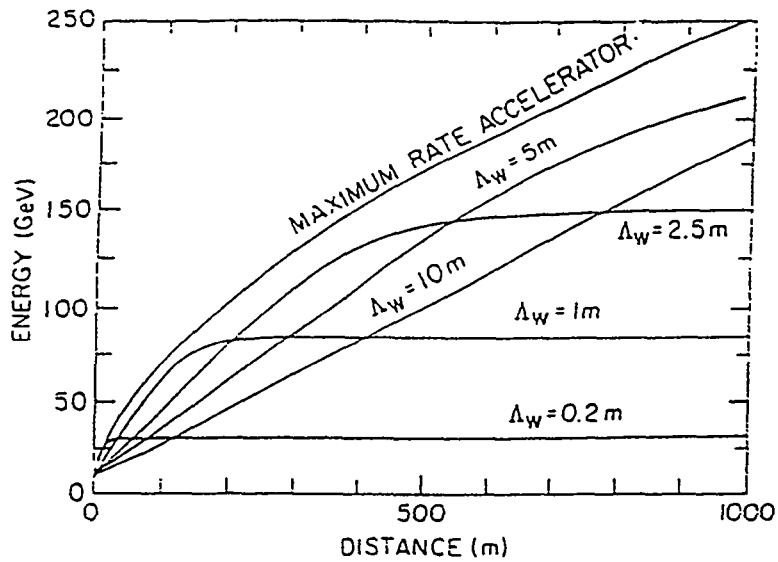

Fig. 3.3 Electron energy versus distance for a constant period IFEL accelerator [76].

Fig. 3.4 shows how the energy varies with distance in a constant field strength accelerator. The energy still saturates, but it takes longer since the radiation losses here are proportional to γ^2. Strong fields give the maximum initial acceleration rate. In both of these cases there is a maximum possible electron energy for a given amount of laser power, independent of the length of the interaction. If it is possible to maintain a constant K , the radiation losses that are proportional to γ^2. Thus for this case the energy does not saturate with distance and at high energy the acceleration rate is proportional to $z^{1/2}$.

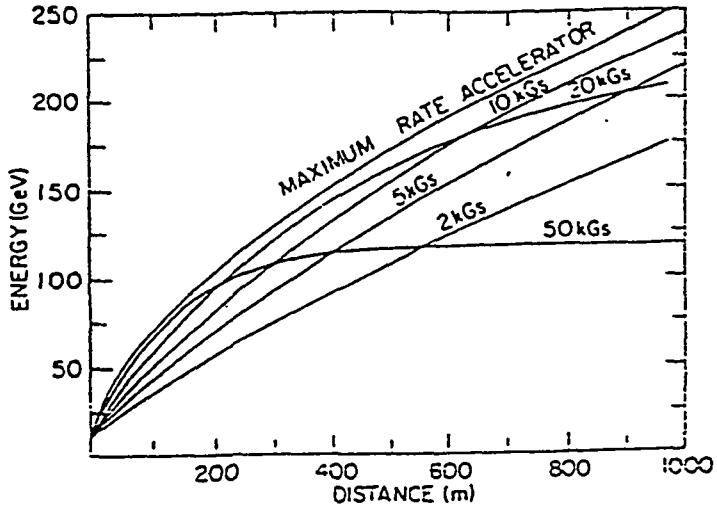

Fig. 3.4 Electron energy versus distance for a constant field strength IFEL accelerator [76].

The longitudinal phase space properties of the electron beam are described using the variables

$$\delta\gamma = \gamma - \gamma_r$$
$$\phi = \psi - \psi_r$$

where the subscript r refers to the resonant values of the quantities. During acceleration the longitudinal phase space $\delta\gamma \bullet \phi$ decreases because of radiation damping. This is an advantage over conventional linear accelerators where $\delta\gamma \bullet \phi$ is approximately constant. Since the phase spread decreases as the energy increases, the resonant phase could be changed to maximize $d\gamma / dz$.

3.3 Early acceleration experiments

Acceleration using the IFEL mechanism has been demonstrated in an experiment at Yerevan Institute in Armenia [79-80]. They used a 12 MeV electron beam from a microtron source together with a 20 MW CO_2 laser. The 20 cm long wiggler had a period of 9.5 mm and field strength of 1 T. The maximum observed energy gain was 20 keV, corresponding to an accelerating gradient of ~ 100 keV / m.

IFEL acceleration experiments have also been carried out at Columbia University [81-82]. A 750 keV electron beam was used. The beam passed through two wigglers. The first wiggler was used as an FEL, which generated the power for the acceleration process. The second 37.5 cm long wiggler, which was used for the IFEL, had a tapered period of 1.8 - 2.25 cm and a field strength of 400 G. Around 40% of the FEL power could be used to accelerate trapped electrons. The measured electron energy spectrum is shown in Fig. 3.5. About 9% of the injected electrons were accelerated to a maximum energy gain of ~ 1 MeV, corresponding to an accelerating gradient of ~ 2.7 MeV / m.

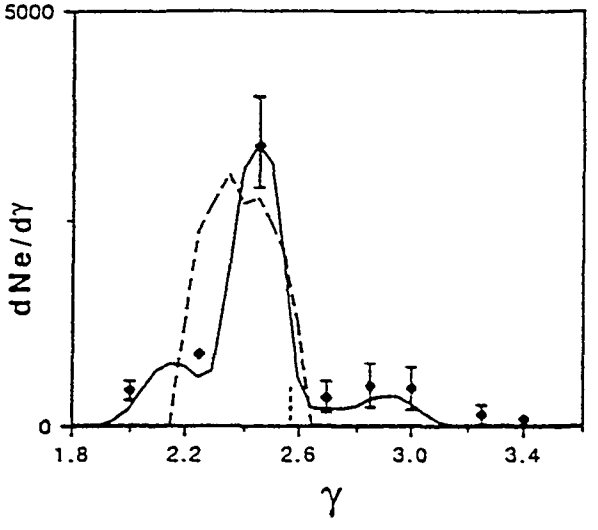

Fig. 3.5 Measured electron energy spectrum for Columbia University IFEL experiment [82].

3.4 Acceleration experiment at BNL

A program of IFEL acceleration studies [83-85] is currently underway at the ATF at BNL. The goals of this program are to build a high energy IFEL demonstration accelerator and to optimize the IFELA as a high current injector for other higher energy accelerators. The IFEL is powered using the ATF CO_2 laser.

The layout of the experiment is shown in Fig. 3.6. In the current run a 45 MeV electron beam will be used. The electron beam optics produce a waist in the center of the wiggler with no dispersion. The betatron focusing parameter $\beta_{\perp X} \approx 1/2\ L_w$ and $\beta_{\perp Y}$ is matched to the

wiggler's natural vertical focusing. The ATF laser will deliver a 5 GW, 50 ps CO_2 pulse to the experiment. The CO_2 light is confined in the wiggler region using a 2.8 mm ID circular. sapphire light guide.

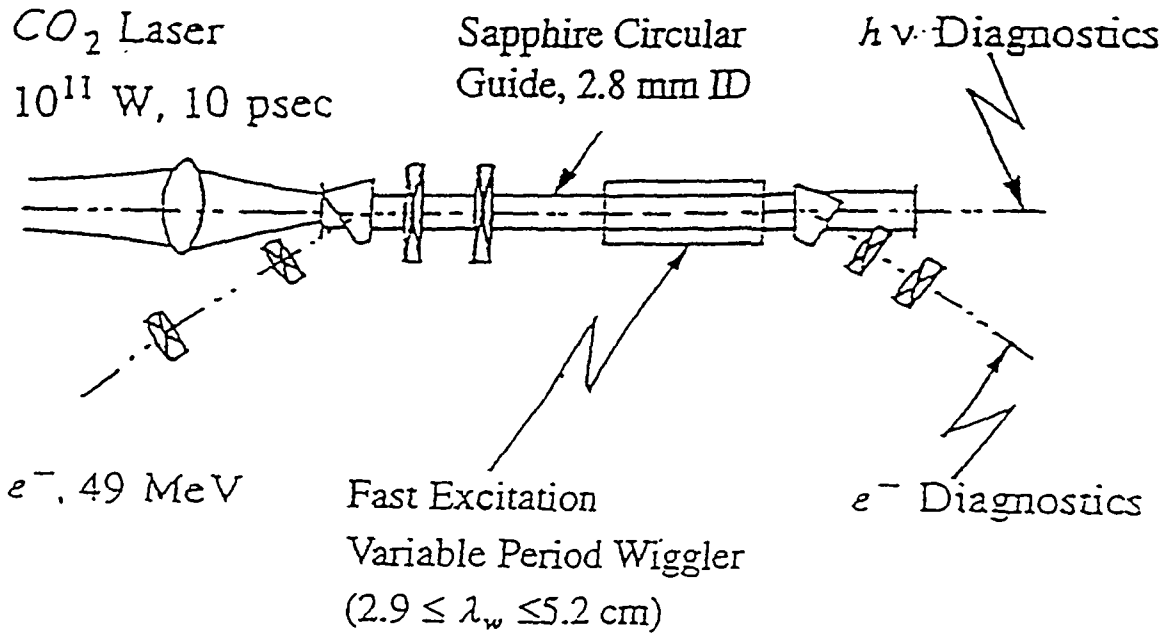

Fig. 3.6 Schematic diagram of the IFEL experiment at BNL [83].

A 0.47 m long pulsed, fast excitation wiggler will be used [86,96]. The period of the wiggler is tapered from 2.9 to 5.2 cm. The field strength is 1.25 T and the pole face gap is 4 mm. The wiggler is constructed from a stack of interleaving, 0.25 mm thick VaP laminations, as shown in Fig. 3.7. The stack is bolted together using tie rods, so altering the period tapering is an easy operation. Four Cu conductors pass through the laminations. The magnet is energized using a 6 kA, 300 μs current pulse. The laminations are assembled in $\Lambda_w / 4$ groups. These are separated by $\Lambda_w / 8$ thick Cu sheets that act as field reflectors and enhance the strength of the magnetic field by ~ 50%, as shown in Fig. 3.8. The taper rate $d \Lambda_w / dz$ ~ 4%. The r.m.s. error in the measured pole tip fields was 0.15%, while the maximum scatter was 1%. Fourier analysis of the field distribution indicated that the first allowed higher harmonic (n = 3) signal was only ~ 3% of the signal power in the fundamental.

A special run was made using a constant period of 1.03 cm and field strength of 0.29 T in the wiggler. Spontaneous radiation was measured from the wiggler at a wavelength of 750 nm.

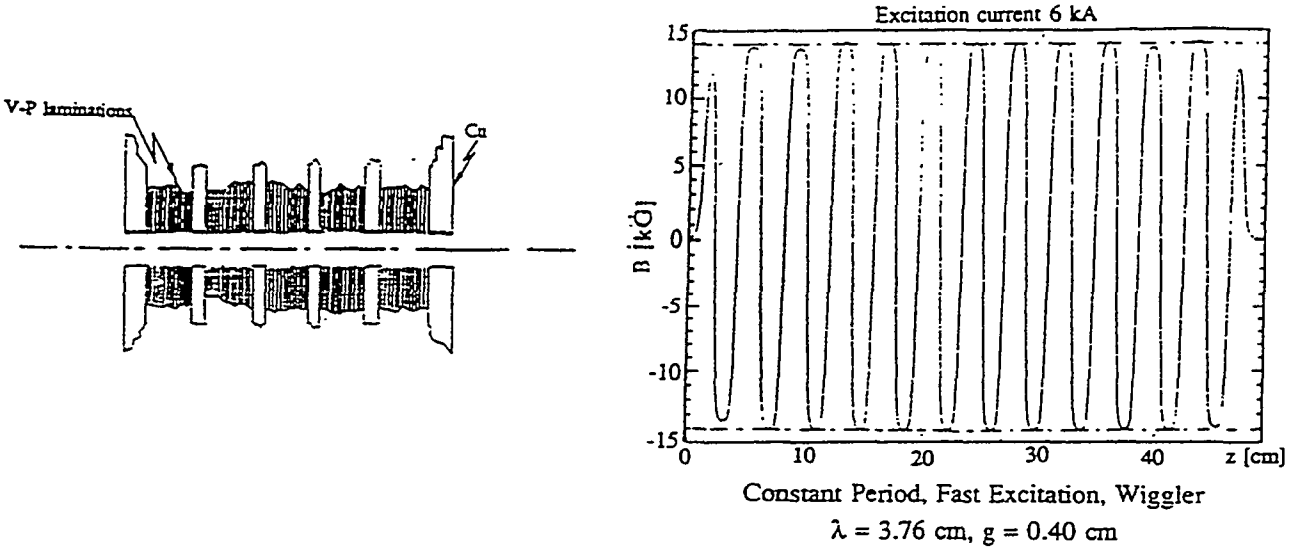

Fig. 3.7 Schematic of wiggler construction and corresponding vertical magnetic field [83].

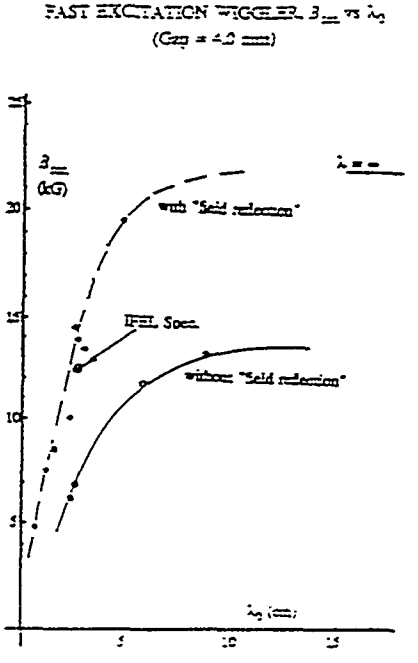

Fig. 3.8 Maximum wiggler magnetic field versus wiggler period [83].

Computer simulations predict a 7 MeV energy gain for the first experiment. About 30% of the incident electrons should be trapped by the interaction and accelerated to the full energy gain. The other electrons should keep the same energy on average, so that at the end of the wiggler the two groups would be cleanly separated in energy.

Near term plans call for increasing the CO_2 laser power delivered to a single IFELA stage to 200 GW. This should give an accelerating gradient of 100 MeV / m. A proposal has been made to build a 100 MeV energy demonstration device by staging 4 of these cells together. A simulation showing the predicted energy gain and clean separation of the accelerated and non-accelerated particles is shown in Fig. 3.9.

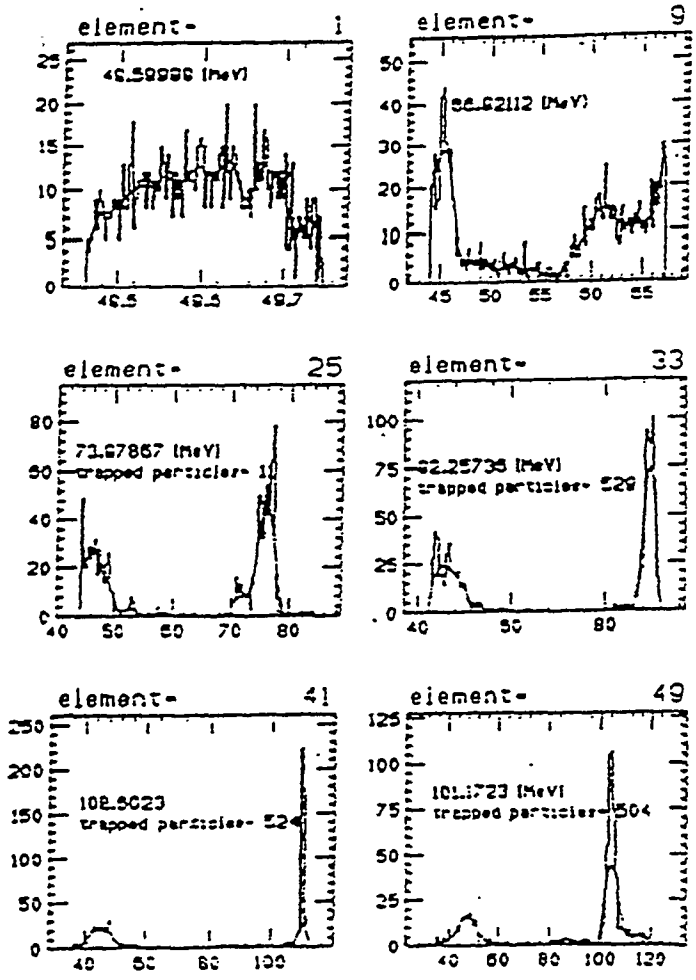

Fig. 3.9 Simulation of 100 MeV IFEL acceleration [83].

3.5 Staging IFELs to higher energy

A number of methods have been proposed to join IFEL sections together into a higher energy accelerator, using:

1. periodic refocusing lenses
2. optical guiding
3. "diffraction-free" optical beams
4. optical waveguides

The first method uses short wiggler sections with $L_W \sim z_R$ separated by refocusing lenses. This system is complex with many parts that need to be aligned. It may be difficult to maintain the tolerances on phase slip. In optical guiding the light is confined inside the electron beam. Calculations indicate that this would only work for an IFEL at low energy [5,87].

Diffraction free optical beams are free space solutions of the wave equation with narrow well-defined radius [88]. For finite dimensions and energies one can only approximate these solutions. The depth of focus is

$$z_{DF} = \frac{2 \pi R}{\alpha \lambda}$$

where R is the radius of the defining aperture and $1 / \alpha$ is the half-width of the central peak. It is possible to have $z_{DF} >> z_R$ if $R >> 1 / \alpha$. Unfortunately, it appears that the diffraction free solutions have a smaller electric field strength in the focus than gaussian beams, so that the net acceleration is about the same.

The optical waveguide reflects the light back and forth inside a hollow tube. The guide adopted for the BNL experiment has a radius of 1 mm, which is 100 times larger than the wavelength of the laser radiation. Significant attenuation would be expected in a guide with metallic walls. The losses occur when the tangential component of the magnetic field is large at a metallic boundary. This can be greatly reduced by using a dielectric waveguide or dielectric coating. Problems involved with using an optical waveguide include coupling of the incident laser beam to the waveguide mode, matching the phase and group velocities, and the creation of parasitic modes. Calculations indicate that the mode transformation occurs over a length $\sim z_R$ and that the production of high order modes should be small. Fig. 3.10 shows measurements of the optical beam radius versus distance for several optical guides. Free space diffraction is also shown for comparison. Measurements with a 2.8 mm diameter sapphire tube showed a power transmission greater than 90% over a distance of 1 m.

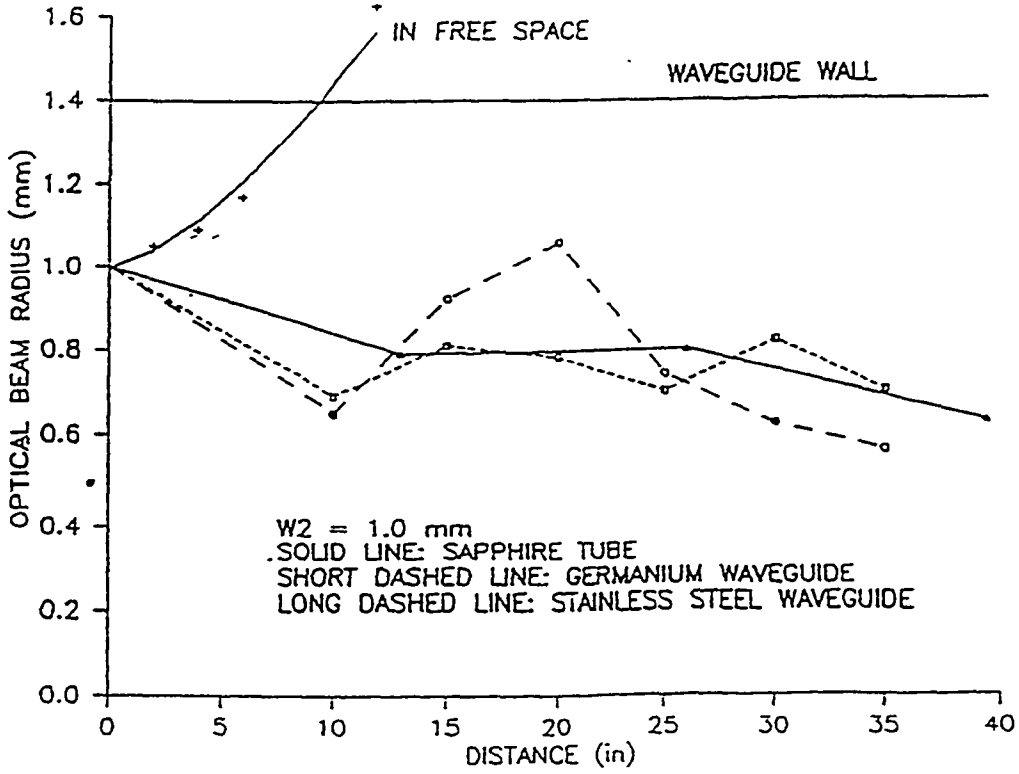

Fig. 3.10 Measurements of optical beam radius as a function of distance [84].

An interesting idea that could be used to reduce the total power requirements with a helical undulator is to use an annular laser beam [78].

3.6 Future directions

Besides the 100 MeV acceleration demonstration mentioned above, several studies have considered the use of an IFEL accelerator as part of a B-factory [89-90].

Acknowledgements

I would like to thank J. Gallardo, R.B. Palmer, and Arie van Steenbergen for useful discussions. This work was supported by the U.S. Department of Energy under contract no. DE-AC02-76CH00016.

References

[1] C. Pellegrini, Report of the working group on far field accelerators, in P.J. Channell (ed), Laser Acceleration of Particles (Los Alamos, NM), AIP Conf. Proc. 91:138-53, 1982.

[2] R.H. Pantell, Interactions between electromagnetic fields and electrons, AIP Conf. Proc. 87:863-918, 1982.

[3] J.D. Lawson & M. Tigner, The physics of particle accelerators, Ann. Rev. Nuc. Part. Sci. 34:99-123, 1984.

[4] C. Joshi, Laser accelerators, IEEE Trans. Nuc. Sci. NS-32:1576-81, 1985.

[5] L.N. Hand, Summary of the working group on novel and exotic ideas, in F.E. Mills (ed), Advanced Accelerator Concepts (Madison, WI), AIP Conf. Proc. 156:395-410, 1986.

[6] A.M. Sessler, The quest for ultrahigh energies, Am. J. Phys. 54: 505-10, 1986.

[7] R.B. Palmer, An introduction to accelerator mechanisms, in Frontiers on Particle Beams South Padre, TX), 1986 and SLAC-PUB-4320, 1987.

[8] C. Tang, Report of the working group on far field accelerators, in J.S. Wurtele (ed), Advanced Accelerator Concepts (Port Jefferson, NY), AIP Conf. Proc. 279:259-69, 1992.

[9] R.B. Palmer, Acceleration theorems, BNL-61317, 1994.

[10] A. Boivin & E. Wolf, Electromagnetic field in the neighborhood of the focus of a coherent beam, Phys. Rev. B138:1561, 1965.

[11] L.D. Landau & E.M. Lifshitz, Classical Theory of Fields, 4th English ed., Pergamon Press, 1975, p. 118.

[12] V.S. Voronin & A.A. Kolomenskii, The pressure of an intense plane wave on a free charge and on a charge in a magnetic field, Sov. Phys. JETP 20:1027-31, 1965.

[13] G.A. Nagorskii & Yu.F. Orlov, Stable motion and acceleration of a charged particle in a linearly polarized electromagnetic wave in a gaseous medium, Sov. Phys. JETP 37:387-9, 1973.

[14] S. Kawata et al, Electromagnetic cross-field acceleration, in C. Joshi (ed), Advanced Accelerator Concepts (Lake Arrowhead, CA), AIP Conf. Proc. 193:172-202, 1989.

[15] S. Kawata et al, Electron acceleration by an electromagnetic wave with a static magnetic field, Part. Acc. 32:229-34, 1990.

[16] V.V. Apollonov et al, Electron acceleration by intense laser beam in a static magnetic field, Sov. Phys. JETP 70:846-52, 1990.

[17] Y.W. Chan, Ultra-intense laser radiation as a possible energy booster for relativistic charged particle, Phys. Lett. 35A:305-6, 1971.

[18] V.V. Apollonov et al, Electron acceleration in stimulated Compton scattering, JETP Lett. 44:75-7, 1986.

[19] M.J. Abedi, Three-wave accelerator and how it compares with two-wave accelerator, in C. Joshi & T. Katsouleas (eds), Laser Acceleration of Particles (Malibu, CA), AIP Conf. Proc. 130:367-73, 1985.

[20] L. Feng & Y. Ho, Net electron acceleration by a strong laser field and rf wave, Phys. Rev. E 49:740-4, 1994.

[21] R.H. Pantell & T.I. Smith, Laser driven electron acceleration by means of two-wave interaction, Appl. Phys. Lett. 40:753-4, 1982.

[22] R.H. Pantell & J.A. Edighoffer, Inverse synchrotron interaction, J. Appl. Phys. 51:1905-8, 1980.

[23] S. Kawata et al, Inverse bremsstrahlung electron accelerator, Phys. Rev. Lett. 66:2072-5, 1991.

[24] M.S. Hussein & M.P. Pato, Nonlinear amplification on inverse bremsstrahlung electron acceleration, Phys. Rev. Lett. 68:1136-9, 1992.

[25] M.S. Hussein, The "NAIBEA" accelerator, in J.S. Wurtele (ed), Advanced Accelerator Concepts (Port Jefferson, NY), AIP Conf. Proc. 279:361-70, 1992.

[26] A.A. Kolomenskii & A.N. Lebedev, Resonance effects associated with particle motion in a plane electromagnetic field, Sov. Phys. JETP 17:179-84, 1963.

[27] C.S. Roberts & S.J. Buchsbaum, Motion of a charged particle in a constant magnetic field and a transverse electromagnetic wave propagating along the field, Phys. Rev. A135:381-9, 1964.

[28] H.R. Jory & A.W. Trivelpiece, Charged particle motion in large amplitude electromagnetic fields, J. Appl. Phys. 39:3053-60, 1968.

[29] W.B. Colson & S.K. Ride, A laser accelerator, Appl. Phys. 20:61-5, 1979.

[30] D.B. McDermott et al, Production of relativistic rotating electron beams by gyroresonant rf acceleration in a TE_{111} cavity, J. Appl. Phys. 58:4501-8, 1985.

[31] A. Loeb & L. Friedland, Autoresonance laser accelerator, Phys. Rev. A 33:1828-35, 1986.

[32] V.V. Apollonov et al, Electron acceleration by intense laser beam in a static magnetic field, Sov. Phys. JETP 70:846-52, 1990.

[33] C. Chen, Prospects and limitations of cyclotron resonance laser acceleration, in J.S. Wurtele (ed), Advanced Accelerator Concepts (Port Jefferson, NY), AIP Conf. Proc. 279:270-5, 1992.

[34] C. Chen, Theory of electron cyclotron resonance laser accelerators, Phys. Rev. A 46:6654-61, 1992.

[35] K.H. Tsui, Electron beam acceleration by cyclotron autoresonance interaction, Phys. Rev. E 51:649-52, 1995.

[36] M.J. Feldman & R.Y. Chiao, Single cycle electron acceleration in focused laser fields, Phys. Rev. A 4:352-8, 1971.

[37] J.K. McIver & M.J. Lubin, On the question of charged particle motion in a focused laser field, J. Appl. Phys. 45:1682-7, 1974.

[38] J.A. Edighoffer & R.H. Pantell, Energy exchange between free electrons and light in vacuum, J. Appl. Phys. 50:6120-2, 1979.

[39] A.A. Varfolomeev & A.H. Hairetdinov, Laser cavities for far field particle acceleration without radiation limits typical for IFEL, in J.S. Wurtele (ed), Advanced Accelerator Concepts (Port Jefferson, NY), AIP Conf. Proc. 279:319-25, 1992.

[40] L.C. Steinhauer & W.D. Kimura, A new approach for laser particle acceleration in vacuum, J. Appl. Phys. 72:3237-45, 1992.

[41] E.J. Bochove et al, Acceleration of particles by an asymmetric Hermite-Gaussian laser beam, Phys. Rev. A 46:6640-53, 1992.

[42] L.C. Steinhauer & W.D. Kimura, Phase control in high gradient laser particle accelerators, in Proc. 1993 Part. Acc. Conf. p. 2581-3.

[43] M.I. Dyakonov & D.A. Varshalovich, Optical modulation of electron beam by inverse Cerenkov effect, Phys. Lett. 35A:277-8, 1971.

[44] A.M. Sessler, Report of the group on media accelerators, in P.J. Channell (ed), Laser Acceleration of Particles (Los Alamos, NM), AIP Conf. Proc. 91:11-27, 1982.

[45] W.D. Kimura, Electron momentum modulation by the stimulated Cerenkov interaction, J. Appl. Phys. 53:5435-9, 1982.

[46] J.R. Fontana & R.H. Pantell, A high energy, laser accelerator for electrons using the inverse Cherenkov effect, J. Appl. Phys. 54:4285-8, 1983.

[47] J.R. Fontana, Inverse Cherenkov acceleration, in C. Joshi & T. Katsouleas (eds), Laser Acceleration of Particles (Malibu, CA), AIP Conf. Proc. 130:357-66, 1985.

[48] K. Shimoda, Proposal for an electron accelerator using an optical maser, Appl. Optics 1:33-5, 1962.

[49] G.A. Nagorskij, Laser acceleration of particles using resonance inversions of the Cherenkov effect, Nuc. Instr. Meth. A248:31-8, 1986.

[50] M.A. Piestrup et al, Momentum modulation of a free electron beam with a laser, J. Appl. Phys. 46:132-7, 1975.

[51] J.A. Edighoffer et al, Observation of inverse Cerenkov interaction between free electrons and laser light, Phys. Rev. A 23:1848-54, 1981.

[52] W.D. Kimura et al, Observation of coherent Cerenkov radiation at optical frequencies, Appl. Phys. Lett. 40:102-4, 1982.

[53] W.D. Kimura et al, The stimulated Cerenkov interaction and its applications, IEEE QE-18:239-45, 1982.

[54] A.S. Fisher et al, Propagation of a picosecond duration, relativistic electron beam through hydrogen at atmospheric pressures, J. Appl. Phys. 64:575-80, 1988.

[55] R.D. Romea & W.D. Kimura, Modeling of inverse Cerenkov laser acceleration with axicon laser beam focusing, Phys. Rev. D 42:1807-18, 1990.

[56] W.D. Kimura et al, Progress on inverse Cerenkov laser accelerator experiment, in C. Joshi (ed), Advanced Accelerator Concepts (Lake Arrowhead, CA), AIP Conf. Proc. 193:203-16, 1989.

[57] W.D. Kimura et al, Update on the ATF inverse Cerenkov laser acceleration experiment, in Proc. 1993 IEEE Part. Accel. Conf., p. 2564-6.

[58] I. Ben-Zvi, The BNL Accelerator Test Facility and experimental program, in Proc. 1991 Part. Acc. Conf. p. 550-4.

[59] I. Ben-Zvi et al, Feed forward RF control system of the Accelerator Test Facility, in Proc. 1991 Part. Acc. Conf. p. 1323-5.

[60] I. Ben-Zvi, The BNL Accelerator Test Facility and experimental program, in J.S. Wurtele (ed), Advanced Accelerator Concepts (Port Jefferson, NY), AIP Conf. Proc. 279:590-607, 1992.

[61] I. Pogorelsky, High power picosecond CO_2 laser system for ATF electron accelerator project, in J.S. Wurtele (ed), Advanced Accelerator Concepts (Port Jefferson, NY), AIP Conf. Proc. 279:608-19, 1992.

[62] H.G. Kirk, Advanced R & D for electron and photon beams at Brookhaven National Laboratory, in M. Month & M. Dienes (eds), The Physics of Particle Accelerators, AIP Conf. Proc. 249:2090-2101, 1992.

[63] X. Wang et al, Intense electron emission due to picosecond laser-produced plasmas in high gradient electric fields, J. Appl. Phys. 72:888-94, 1992.

[64] K. Batchelor et al, Performance of the Brookhaven photocathode rf gun, Nuc. Instr. Meth. A318:372-6, 1992.

[65] X. Wang et al, Automatic emittance measurement at the ATF, in Proc. 1993 Part. Acc. Conf. p. 2486-8.

[66] X. Wang et al, Design and construction of a full copper photocathode RF gun, in Proc. 1993 Part. Acc. Conf. p. 3000-2.

[67] K. Batchelor et al, Operational experience on the Brookhaven National Laboratory Accelerator Test Facility, Proc. 4th European Acc. Conf. , p. 736-8, 1994.

[68] W.D. Kimura et al, Laser acceleration of relativistic electrons using the inverse Cherenkov effect, Phys. Rev. Lett. 74:546-9, 1995.

[69] S.C. Tidwell et al, Generating radially polarized beams interferometrically, Appl. Optics 29:2234-9, 1990.

[70] S.C. Tidwell et al, Transporting and focusing radially polarized laser beams, Optical Eng. 31:1527-31, 1992.

[71] S.C. Tidwell et al, Efficient radially polarized laser beam generation using a double interferometer, Appl. Optics 32:5222-9, 1993.

[72] R.B. Palmer, Interaction of relativistic particles and free electromagnetic waves in the presence of a static helical magnet, J. Appl. Phys. 43:3014-23, 1972.

[73] H. Motz, Undulators and free electron lasers, Contemp. Phys. 20:547-68, 1979.

[74] P. Sprangle & C-M. Tang, Laser beat wave electron accelerator, IEEE NS-28:3346-8, 1981.

[75] C. Pellegrini & I.E. Campisi, The inverse free electron laser accelerator, in M. Month (ed), Physics of High Energy Particle Accelerators, AIP Conf. Proc. 105:1058-1102, 1983.

[76] E.D. Courant et al, High-energy inverse free-electron-laser accelerator, Phys. Rev. A32:2813-23, 1985.

[77] E.D. Courant et al, High-energy inverse free-electron-laser accelerator, in M. Month et al (eds), Physics of High Energy Particle Accelerators, AIP Conf. Proc. 127:849-74, 1985.

[78] M.A. Piestrup & J.A. Edighoffer, A gas loaded transverse field accelerator, in C. Joshi & T. Katsouleas (eds), Laser Acceleration of Particles (Malibu, CA), AIP Conf. Proc. 130:329-44, 1985.

[79] A.T. Amatuni et al, Development of new methods for charged particle acceleration at Yerevan Physics Instutute, internal report, 1989.

[80] A.T. Amatuni et al, Development of new methods for charged particle acceleration at Yerevan Physics Instutute, Part. Accel. 32:221-7, 1990.

[81] T.C. Marshall et al, Inverse FEL accelerator: experiment and theory, Nuc. Instr. Meth. A304:683-6, 1991.

[82] I. Wernick & T.C. Marshall, An inverse free electron laser accelerator experiment, in J.S. Wurtele (ed), Advanced Accelerator Concepts (Port Jefferson, NY), AIP Conf. Proc. 279:292-8, 1993.

[83] A. Fisher, J. Gallardo, J. Sandweiss & A. van Steenbergen, Inverse free electron laser accelerator, in J.S. Wurtele (ed), Advanced Accelerator Concepts (Port Jefferson, NY), AIP Conf. Proc. 279:299-318, 1993.

[84] A.S. Fisher et al, An inverse free electron laser accelerator, in Proc. 1993 IEEE Part. Accel. Conf., p. 2578-80.

[85] A. Fisher et al, Inverse free electron laser accelerator development, Nuc. Instr. Meth. A341: ABS 111, 1994. (abstract)

[86] A. van Steenbergen et al, Fast excitation variable period wiggler, in Proc. 1991 IEEE Part. Accel. Conf., p. 2724-6.

[87] A.A. Varfolomeev & A.H. Hairetdinov, Optical guiding in inversed FEL, in J.S. Wurtele (ed), Advanced Accelerator Concepts (Port Jefferson, NY), AIP Conf. Proc. 279:330-7, 1993.

[88] S.Y. Cai et al, "Diffraction free" optical beams in inverse free electron laser accelerators, Nuc. Instr. Meth. A272:481-4, 1988.

[89] C. Pellegrini et al, Use of an inverse free electron laser in a linear collider B factory, in J.S. Wurtele (ed), Advanced Accelerator Concepts (Port Jefferson, NY), AIP Conf. Proc. 279:338-52, 1993.

[90] N. Barov et al, An inverse free electron laser driven linear collider electron-positron B-factory, in Proc. 1993 IEEE Part. Accel. Conf., p. 2617-9.

[91] L.C. Steinhauer & W.D. Kimura, High-γ inverse Cerenkov acceleration in resonant media, J. Appl. Phys. 68:4929-36, 1990.

[92] L.C. Steinhauer & W.D. Kimura, Multistaging and e-beam trapping in laser particle accelerators, in J.S. Wurtele (ed), Advanced Accelerator Concepts (Port Jefferson, NY), AIP Conf. Proc. 279:539-50, 1992.

[93] J.R. Fontana et al, Design analysis for a 100 MeV inverse Cerenkov laser accelerator, in Proc. 1993 IEEE Part. Accel. Conf., p. 2614-6.

[94] P.J. Channell et al, Laser focusing of particle beams, in C. Joshi & T. Katsouleas (eds), Laser Acceleration of Particles (Malibu, CA), AIP Conf. Proc. 130:407-20, 1985.

[95] P.J. Channell, Laser focusing of high energy, charged particle beams, in F.E. Mills (ed), Advanced Accelerator Concepts (Madison, WI), AIP Conf. Proc. 156:519-30, 1986.

[96] A. van Steenbergen, Patent application 368618, June 1989 (issued August 1990).

[97] W.D. Kimura et al, Inverse Cerenkov acceleration and scaling to TeV accelerators, Particle World 4:22-31, 1995.